Quantum chemical study on influence of intermolecular hydrogen bonding on the geometry, the atomic charges and the vibrational dynamics of 2,6-dichlorobenzonitrile

ARTICLE *in* SPECTROCHIMICA ACTA PART A MOLECULAR AND BIOMOLECULAR SPECTROSCOPY · NOVEMBER 2013

Impact Factor: 2.35 · DOI: 10.1016/j.saa.2013.10.104 · Source: PubMed

7 AUTHORS, INCLUDING:

Archana Gupta
M.J.P. Rohilkhand University
24 PUBLICATIONS **118** CITATIONS
SEE PROFILE

Poonam Tandon
University of Lucknow
206 PUBLICATIONS **986** CITATIONS
SEE PROFILE

Soni Mishra
University College London
25 PUBLICATIONS **117** CITATIONS
SEE PROFILE

Spectrochimica Acta Part A: Molecular and Biomolecular Spectroscopy 121 (2014) 464–482

Contents lists available at ScienceDirect

Spectrochimica Acta Part A: Molecular and Biomolecular Spectroscopy

journal homepage: www.elsevier.com/locate/saa

Quantum chemical study on influence of intermolecular hydrogen bonding on the geometry, the atomic charges and the vibrational dynamics of 2,6-dichlorobenzonitrile

Parag Agarwal [a], Saba Bee [b], Archana Gupta [b,*], Poonam Tandon [a], V.K. Rastogi [c], Soni Mishra [d], Poonam Rawat [e]

[a] Department of Physics, Lucknow University, Lucknow, India
[b] Department of Applied Physics, Faculty of Engineering & Technology, M.J.P. Rohilkhand University, Bareilly, India
[c] Aryan Institute of Technology, Ghaziabad, India
[d] Department of Inorganic and Physical Chemistry, Indian Institute of Science, Bangalore, India
[e] Department of Chemistry, Lucknow University, Lucknow, India

HIGHLIGHTS

- FT-IR and FT-Raman spectra of 2,6-dichlorobenzonitrile have been recorded.
- Spectra are simulated by DFT for monomer and tetramer forms using optimized geometry.
- NBO analysis has been done for the interpretation of hyperconjugative interactions.
- The effects of BSSE on vibrational wavenumbers are discussed.
- The excited-state hydrogen bond effects on vibrational spectra have been discussed.

GRAPHICAL ABSTRACT

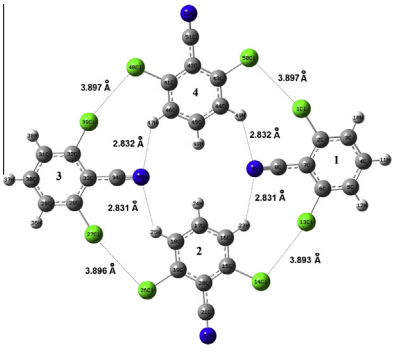

ARTICLE INFO

Article history:
Received 25 June 2013
Received in revised form 23 October 2013
Accepted 31 October 2013
Available online 7 November 2013

Keywords:
Vibrational spectroscopy
DFT
Intermolecular interactions
BSSE
Excited state dynamics

ABSTRACT

FT-IR (4000–400 cm^{-1}) and FT-Raman (4000–200 cm^{-1}) spectral measurements on solid 2,6-dichlorobenzonitrile (2,6-DCBN) have been done. The molecular geometry, harmonic vibrational frequencies and bonding features in the ground state have been calculated by density functional theory at the B3LYP/6-311++G (d,p) level. A comparison between the calculated and the experimental results covering the molecular structure has been made. The assignments of the fundamental vibrational modes have been done on the basis of the potential energy distribution (PED). To investigate the influence of intermolecular hydrogen bonding on the geometry, the charge distribution and the vibrational spectrum of 2,6-DCBN; calculations have been done for the monomer as well as the tetramer. The intermolecular interaction energies corrected for basis set superposition error (BSSE) have been calculated using counterpoise method. Based on these results, the correlations between the vibrational modes and the structure of the tetramer have been discussed. Molecular electrostatic potential (MEP) contour map has been plotted in order to predict how different geometries could interact. The Natural Bond Orbital (NBO) analysis has been done for the chemical interpretation of hyperconjugative interactions and electron density transfer between occupied (bonding or lone pair) orbitals to unoccupied (antibonding or Rydberg) orbitals. UV spectrum was measured in methanol solution. The energies and oscillator strengths were calculated by Time Dependent Density Functional Theory (TD-DFT) and matched to the experimental findings. TD-DFT method has also been used for theoretically studying the hydrogen bonding dynamics by monitoring the spectral shifts of some characteristic vibrational modes involved in the formation of

* Corresponding author. Tel.: +91 9411922252.
E-mail address: drarchana.physics@gmail.com (A. Gupta).

http://dx.doi.org/10.1016/j.saa.2013.10.104

hydrogen bonds in the ground and the first excited state. The ^{13}C nuclear magnetic resonance (NMR) chemical shifts of the molecule were calculated by the Gauge independent atomic orbital (GIAO) method and compared with experimental results. Standard thermodynamic functions have been obtained and changes in thermodynamic properties on going from monomer to tetramer have been presented.

Introduction

Benzonitrile (BN) and its derivatives have been studied extensively because of their wide applications in various fields [1–4]. Benzonitrile is used as an extraction solvent for fatty acids, oils and unsaturated hydrocarbons; chemical intermediate for the synthesis of pharmaceuticals, dyestuffs and rubber. Fluorinated benzonitrile compounds are widely used in industry as heat transfer fluids. 3-ethyl benzonitrile is used for the treatment of urge urinary in continence (UUI) [5], while *p*-hydroxy benzonitrile has alpha blocker properties on the cardiovascular system of rates [6]. Due to the high electro-negativity of chlorine atom, entirely different physical and chemical properties of chlorobenzonitrile derivatives are observed as compared to the other halogenated compounds. 3-chlorobenzonitrile and 4-chlorobenzonitrile are used for inhibition of hydrogen absorption. Dihalogenated benzonitrile analogs are active compounds in a number of herbicides. 2,6-dichlorobenzonitrile (2,6-DCBN) is a contact herbicide which controls broadleaf weeds in grass type crops and in cranberry bogs [7]. It is among the most toxic chemical to nasal tissue. Damage to this reduces smelling ability [8] and the transport of an important amino acid to the brain. It is a cellulose synthesis inhibitor. It has also been used as a tool for investigating cell wall assembly and stress [9]. It is persistent in water and soil. 2,6-DCBN is a valuable intermediate for preparing a series of highly efficient pesticides. e.g. 2,6-difluoro benzamide, a fluorinated derivative of DCBN, is used to synthesize benzyl urea like pesticides. Many other agricultural chemicals such as chlorfluazuron, flufenoxuron, flucycloxuron, hexaflumuron, diflubenzuron, teflubenzuron etc. [10] are also prepared from 2,6-DCBN. In addition, it is used to prepare "polyphenyl ether hydrocyanic ester" which bears high heat resistant properties among all other thermoplastics. In many countries, the usage of 2,6-DCBN and the problems associated with groundwater contamination by its main degradation product 2,6-dichlorobenzamide have resulted in intensive research and monitoring of these compounds. Thus, 2,6-DCBN is expected to be promising for the future of its marketing value.

The solid-state properties of compounds are mainly directed by the intermolecular hydrogen bond forces. Intermolecular hydrogen bond determines the processes of complexing, ordering of the physical structure, and crystallization, mutual packing of molecules in solids, and the form of molecular objects. Weak intermolecular interactions significantly contribute to the reactivity and biological activity of the molecule. Vibrational spectroscopy has found wide application in the study of weak intermolecular interactions, especially in the case of hydrogen and ionic bonds. DFT calculations have been applied to study structural behavior of materials at molecular level, thus to aid interpretation of spectroscopic experimental data. Vibrational spectra of benzonitrile and many of its mono- and di- substituted derivatives have been studied [11–13], yet no detailed theoretical and experimental vibrational analysis on 2,6-DCBN has been reported. In continuation of our work on a variety of molecules [14–17], the present investigation has been undertaken to study the vibrational spectra of this important molecule completely and to identify the normal modes of vibration with the help of density functional theory. We have determined the molecular structure, harmonic vibrational wavenumbers, absolute Raman scattering activities and infrared absorption intensities of the title compound. Simulations in the tetramer form have been done to study the effect of intermolecular interactions. In addition, the infrared spectra of the electronically excited state of the hydrogen-bonded tetramer are also calculated using TD-DFT to monitor the spectral shifts of the vibrational modes most likely involved in the formation of intermolecular hydrogen bonds.

Experimental details

The compound 2,6-DCBN of spectral grade in solid state was purchased from M/s Aldrich Chemical Company (USA) and used as such without further purification. The infrared spectra were recorded with Bruker ALPHA FT-IR Spectrometer using ATR module in the region 4000–400 cm^{-1}. For the spectra 256 scans were collected at 3 cm^{-1} resolution.

The FT-Raman spectra of 2,6-DCBN were recorded in powder form in the region 4000–200 cm^{-1} on a Bruker MultiRAM spectrometer. The NIR output (1064 nm) of a Nd:YAG laser was used to excite the spectrum. The laser power was set at 5 mW and the spectra were recorded over 512 scans at a fixed temperature. The spectral resolution was 4.0 cm^{-1}.

Differential scanning calorimetry was performed using a Mettler Toledo DSC calorimeter operating with Stare software. The sample was encapsulated in an aluminum pan having pierced lid to allow escape of volatiles. The temperature range was 25–160 °C, with a heating rate of 5 °C min^{-1}. Nitrogen purge at 30 ml min^{-1} was employed. The calorimeter was calibrated using indium standard. The experimental data are shown in Fig. 1.

The ultraviolet absorption spectra of 2,6-DCBN were examined in the range 200–500 nm using a Shimadzu UV 1800 Spectrophotometer. The UV pattern is taken from a 10^{-5} M solution prepared by dissolving 2,6-DCBN in methanol solvent. The experimental UV–vis spectra are shown in Fig. 2.

The ^{13}C NMR spectra were recorded on a Bruker DRX-300 spectrometer. The measurements were done in acetone solution

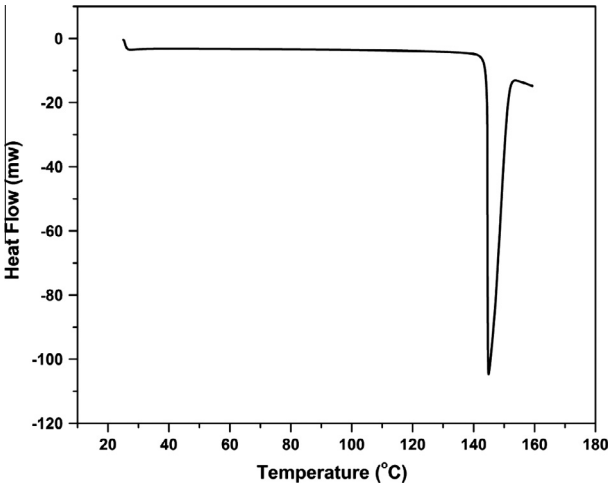

Fig. 1. Differential scanning calorimetry (DSC) thermograph of 2,6-DCBN.

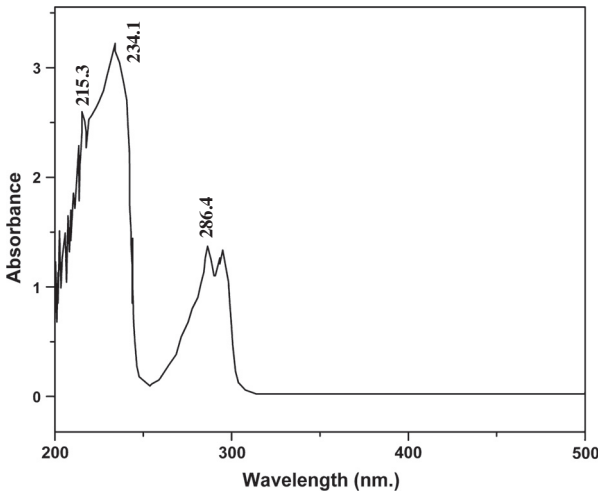

Fig. 2. Experimental UV spectra of 2,6-DCBN in methanol solution.

operating at 300 MHz at 22.6 °C. The solution was prepared by dissolving about 30 mg of the sample in 0.6 mL of acetone. The spectra have following experimental parameters: number of scans 2048; spectral width 18939.395 Hz; acquisition time 1.73 s. Chemical shifts were reported in ppm relative to TMS. The experimental ^{13}C NMR spectra are shown in Fig. 3.

Computational details

The theoretical calculations were performed using the Gaussian 03 software package [18], invoking gradient geometry optimization [19]. The geometry optimization was carried out using density functional theory calculations employing 6-311++G(d,p) basis set and Becke's three parameter (local, nonlocal, Hartree–Fock) hybrid exchange functionals with Lee–Yang–Parr correlation functional (B3LYP) [20–23]. The optimized structural parameters were used in the vibrational frequency calculations within the harmonic approximation at the same level of theory used for the optimized geometry. The absolute Raman scattering and infrared absorption intensities associated with each normal mode, were calculated from the derivatives of the polarizability and dipole moment respectively. The Raman activities were converted into relative Raman intensities using the following relationship derived from the theory of Raman scattering [24,25]:

$$I_i = \frac{f(v_o - v_i)^4 S_i}{v_i[1 - e^{hcv_i/kT}]} \quad (1)$$

where υ_o is the exciting frequency in cm^{-1}, υ_i is the vibrational wavenumber of the ith normal mode, h, c and k are the fundamental constants and f is a suitably chosen common normalization factor for all peak intensities. The normal coordinate analysis was performed and the potential energy distribution (PED) was calculated for the molecule among symmetry coordinates using the program GAR2PED [26]. For this purpose a complete set of 33 symmetrized internal coordinates was defined with help of Pulay's recommendations [27,28]. The vibrational assignments of the normal modes were provided on the basis of the PED. Visualization and checking of calculated data were done by using the Gauss View program [29].

It is well known that the harmonic frequencies by DFT calculations are usually higher than the corresponding experimental quantities due to the fact of the electron correlation approximate treatment, anharmonicity effects and basis set deficiencies, etc. [30], they were scaled down by the wavenumber linear scaling procedure (WLS) of Yoshida et al. [31] [$\upsilon_{obs} = (1.0087–0.0000163\upsilon_{cal})\ \upsilon_{cal}$ cm^{-1}].

Result and discussion

Geometry optimization and conformational analysis

Single crystal XRD studies [32] indicate that the title compound is isomorphous, with two half molecules in the asymmetric unit of a monoclinic unit cell in the space group C2/m. The lattice parameters are: a = 18.0525 (8) Å, b = 20.7374 (10) Å, c = 3.8334 (2) Å, β = 101.143 (1)°. The molecules are packed into layers parallel to (2 0 1) plane. The layers are 3.244 Å apart. They are not exactly planar. The molecules are slightly tilted with respect to the mean layer. Within the layers, the strong (short) intermolecular contacts are H···N and Cl···Cl. Both the H···N and Cl···Cl distances (2.691

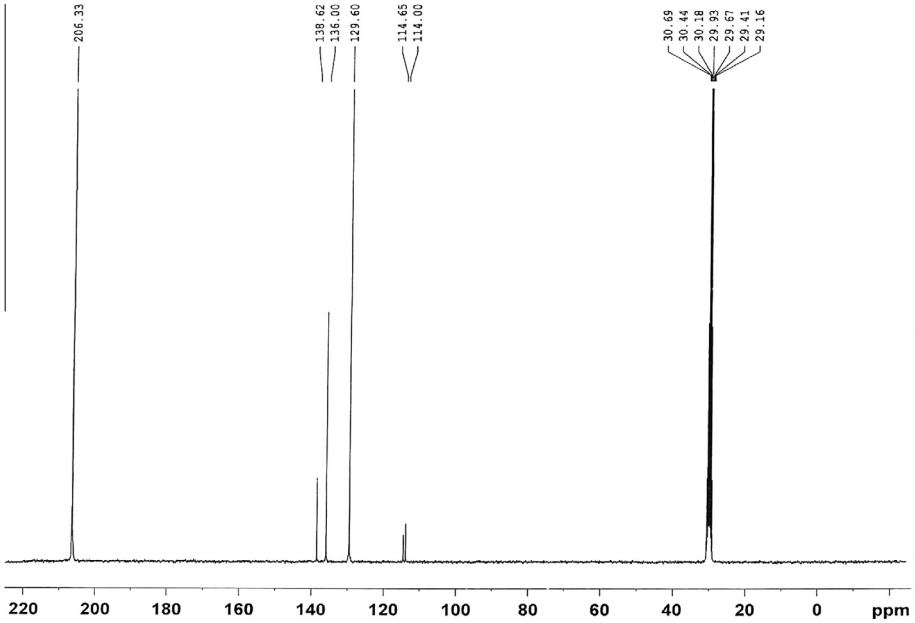

Fig. 3. Experimental ^{13}C NMR spectra of 2,6-DCBN.

and 3.596 Å) are around the usual van der Waals distances (2.75 and 3.5 Å respectively). These shorter distances imply stronger interactions and presumably contribute to the near planarity of the overall arrangement.

Initial geometry generated from single crystal XRD data was minimized without any constraint to the potential energy surface. The optimized structural parameters of 2,6-DCBN in the isolated state are given in Table 1. The optimized molecular structure of the compound with atom numbering scheme adopted in the computation is shown in Fig. 4. It is seen from the table that the benzene ring appears slightly distorted from the regular hexagonal structure. This is due to the effect of substitution of hydrogens with chlorine and cyno group on the phenyl ring. As in case of 2,6-difluorobenzonitrile [33], the ring parameters in 2,6-DCBN also, can be reasonably explained by the superposition of meta-dichlorobenzene [34] and benzonitrile [35] and are shown in Table S1.

The vibrational spectra of the sample have been recorded in the solid state whereas the calculations have been done on the isolated molecule. The effect of intermolecular interactions can be evaluated from the comparison of the molecular properties in the solid state with those referred to the isolated molecule. For this, we need to do calculations in the unit cell. Due to our limited computational facilities, we have considered two types of tetramer models, in which different types of interactions have been taken into account. Accordingly, the structures of two tetramers A and B were optimized at B3LYP/6-31G level. The optimized structures are shown in Fig. 5(a) and (b). The optimized structure of tetramer A gave a good match with the experimental geometry whereas tetramer B showed a large deviation. Hence the whole discussion is based on tetramer A. The frequency calculations were done using the structure of tetramer A optimized at B3LYP/6-311++G(d,p) level.

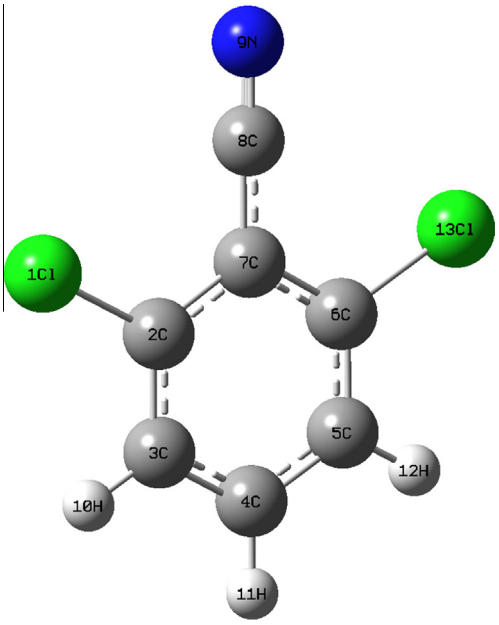

Fig. 4. Optimized structure of 2,6-DCBN monomer.

Table 1
Optimized geometrical parameters of 2,6-DCBN monomer and tetramer A by B3LYP/6-311++G(d,p) in comparison with XRD data.

Geometrical parameters	Optimized monomer	Optimized tetramer A	XRD	Geometrical parameters	Optimized monomer	Optimized tetramer A	XRD
Bond length (Å)				Bond angles (°)			
C2—C7	1.4085	1.4085	1.400	C4—C3—H10	120.98	121.03	120.47
C2—C3	1.3890	1.3886	1.382	C3—C4—H11	119.54	119.03	119.19
C3—C4	1.3915	1.3918	1.382	C5—C4—H11	119.54	119.50	119.19
C4—C5	1.3915	1.3918	1.382	C4—C5—H12	120.98	121.03	120.47
C5—C6	1.3890	1.3886	1.382	C6—C5—H12	119.61	119.58	120.59
C6—C7	1.4088	1.4085	1.400	C7—C6—Cl 13	119.87	119.78	118.94
C7—C8	1.4271	1.4264	1.437	C7—C2—Cl 1	119.75	119.78	118.94
C6—Cl 13	1.7430	1.7427	1.732	C3—C2—Cl 1	119.13	119.21	119.84
C2—Cl 1	1.7429	1.7427	1.732	C5—C6—Cl 13	119.10	119.21	119.84
C3—H10	1.0817	1.0816	0.950	C2—C3—H10	119.60	119.58	120.59
C4—H11	1.0835	1.0835	0.951	Bond Torsions (°)			
C5—H12	1.0817	1.0817	0.951	C7—C2—C3—C4	0.00	0.00	−0.50
C8≡N9	1.1547	1.1551	1.148	C2—C3—C4—C5	0.00	0.00	−0.38
Bond angles (°)				C3—C4—C5—C6	0.00	0.00	0.38
C2—C7—C6	118.09	118.21	118.07	C4—C5—C6—C7	0.01	0.00	−0.14
C6—C7—C8	120.99	120.89	120.96	C2—C7—C8≡N9	−149.83	−48.74	−89.71
C2—C7—C8	121.00	120.90	120.96	C6—C7—C8≡N9	30.17	131.26	89.71
C7—C6—C5	121.13	121.01	121.22	C6—C7—C2—Cl 1	179.99	−179.99	178.26
C2—C3—C4	119.24	119.39	118.94	C2—C7—C6—Cl 13	−180.00	179.99	178.26
C6—C5—C4	119.41	119.39	118.94	C7—C2—C3—H10	−180.00	179.99	179.50
C3—C4—C5	120.92	120.99	121.61	C2—C3—C4—H11	180.00	−179.99	179.64
C7—C2—C3	121.12	121.01	121.22	C3—C4—C5—H12	−180.00	−179.99	−179.62
C7—C8≡N9	179.97	179.99	179.51				
Intermolecular parameters							
Bond length (Å)				Bond angles (°)			
N9···H23		2.8315	2.691	C16—H23···N9		138.37	133.34
N35···H25		2.8315	2.691	C18—H25···N35		138.39	133.34
N35···H47		2.8321	2.691	C46—H47···N35		138.37	133.34
N9···H49		2.8322	2.691	C44—H49···N9		138.39	133.34
Cl 13···Cl 14		3.8962	3.596	C6—Cl 13···Cl 14		164.15	162.69
Cl 26···Cl 27		3.8959	3.596	C19—Cl 26···Cl 27		164.14	162.69
Cl 39···Cl 40		3.8968	3.596	C32—Cl 39···Cl 40		164.14	162.69
Cl 50···Cl 1		3.8967	3.596	C43—Cl 50···Cl 1		164.14	162.69

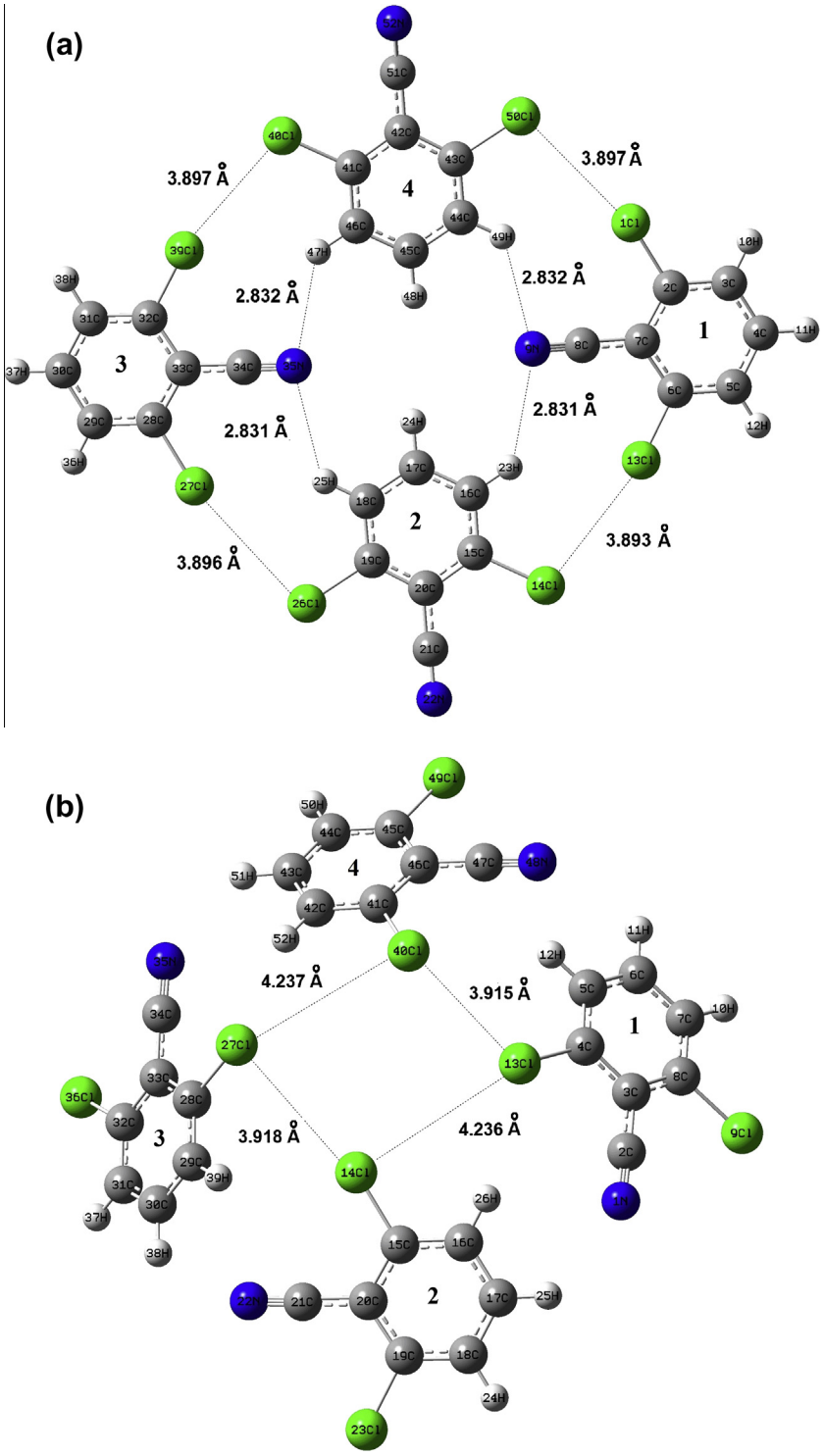

Fig. 5. (a) Optimized structure of 2,6-DCBN tetramer A. (b) Optimized structure of 2,6-DCBN tetramer B.

In the isolated state, the molecule is completely planar as the torsional angles X—C—C—C (X = Cl, H), are 180°. However, small deviations from the planarity are observed in the tetramer due to intermolecular interactions. The intermolecular bond length N9···H23 in tetramer A (2.8315, 2.8315, 2.8321 and 2.8322 Å) is in accordance with corresponding crystal data, 2.691 Å. Another bond length Cl 13···Cl 14 is calculated at 3.8962, 3.8959, 3.8968 and 3.8967 Å in tetramer A and gives a good match with the experimental value at 3.696 Å. The computed value of intermolecular crystal angle C16—H23···N9 for tetramer A, 138.37°, 138.39°, 138.37°, 138.39° differs with that of crystal data at 133.34°. It is due to the crystal forces that give rise to a more packed structure than in our simulation. By contrast, the angle C6—Cl 13···Cl 14 obtained theoretically at 164.15°, 164.14°, 164.14° and 164.14° is in compliance with single crystal XRD data at 162.69°. The calculated length of C≡N bond in two subunits of tetramer A (1.1549 Å), which are not hydrogen bonded, is close to that of monomer (1.1547 Å) whereas in other two subunits the bond length

(1.1551 Å) shows much deviation. As the Cl···Cl contacts can be described as Lewis acid Cl interacting with Lewis base Cl [32], the C—Cl bond lengths in two subunits of the tetramer have been elongated (1.7478 Å), while two have been shortened (1.7426 Å) as compared to that in the isolated state (1.7430 Å).

As can be seen from Table 1, the values of geometrical parameters for the tetramer A are closer to the experimental values as compared to those for the isolated state. The difference in the computed and the experimental values of the tetramer may be attributed to the incorporation of incomplete intermolecular interactions. As we could not simulate all the interactions well, our calculated geometric data appear close to the crystal but do not match exactly.

Natural population analysis

Natural population analysis (NPA) data of monomer and tetramer were used to investigate the changes in charge, which give some insight into the interaction taking place upon aggregation. For the sake of comparison, the calculated natural charges for the monomer and the tetramer of 2,6-DCBN along with the monomer of BN are presented in Table S2. The charge distribution structures of 2,6-DCBN and BN monomer are shown in Fig. S1. As seen from Table S2, significant changes are observed in the charges of the atoms involved in intermolecular interactions.

It is noticed, that all the aromatic ring carbons in BN have negative charge. In 2,6-DCBN, the substitution of hydrogen atoms of the aromatic ring by chlorine group leads to a redistribution of electron density. The charges C2 and C6 atoms which are negative in BN molecule become positive on chlorine substitution in 2,6-DCBN. The carbon atom attached to nitrogen atom (C8) is electron-deficient atom *i.e.* it possesses positive electronic charge due to electronegative character of nitrogen.

The electronegative charges on N9 and N35 atoms increase by 0.04144e and 0.04270e respectively whereas electropositive charges on atoms H23, H25, H47 and H49 increase by 0.00834e, 0.00853e, 0.00860e and 0.00830e respectively on going from monomer to tetramer. The higher partial charges on the atoms in tetramer as compared to those of monomer, suggested a substantial electrostatic interaction, which stabilizes the tetramer species.

The charges on chlorine atoms Cl 1, Cl 13, Cl 27 and Cl 39 increase while on Cl 14, Cl 26, Cl 40 and Cl 50 decrease as compared to monomer values, indicating that the former ones act as Lewis acid and the later ones as Lewis base in the Cl···Cl intermolecular contacts. This observation is further supported by the fact that the angle C—Cl···Cl at the acidic chlorine atom is ∼164° and the angle Cl···Cl—C at the basic chlorine atom is ∼105° [32].

NBO analysis

Natural Bond Orbital (NBO) analysis is one of the most powerful tools for interpreting quantum-chemical results in terms of chemically significant terms. This method localizes the molecular wave functions in optimized electron pairs, corresponding to lone pairs; core pairs on bonding units; giving a picture which is close to the familiar Lewis picture of molecular structure. NBO analysis has been used to identify and confirm the possible intra- and intermolecular interactions between the units of the tetramer. In order to understand various second order interactions between the filled orbitals of one subsystem and vacant orbitals of another subsystem, the NBO calculations were performed using NBO 3.0 program [36] as implemented in the Gaussian 03W package at the DFT/B3LYP/6-311++G(d,p) level.

For each donor (i) and acceptor (j), the stabilization energy $E^{(2)}$ associated with the delocalization $i \rightarrow j$ is estimated as

$$E^{(2)} = \Delta E_{ij} = q_i \frac{F(i,j)^2}{\varepsilon_j - \varepsilon_i} \quad (2)$$

where q_i is the donor orbital occupancy, ε_i and ε_j are diagonal elements and $F(i,j)$ is the off diagonal NBO Fock or Kohn–Sham matrix element [37].

The stabilization energies $E(2)$ are proportional to the NBO interaction intensities. Notwithstanding the fact that the energetic contribution of hyperconjugative interaction is weak, the $E(2)$ values are chemically significant and are used as a measure of the intermolecular delocalization. With greater $E(2)$, i has a greater tendency to provide an electron to j and the degree of electron delocalisation is greater.

Table 2 summarizes the second-order perturbative estimates of "donor–acceptor" (bond–antibond) interactions in the NBO basis for the tetramer A. The intramolecular hyperconjugative interactions are formed by the orbital overlap between σ and π electrons of (C—C) bonds and antibonds. This results in Intra molecular charge transfer, causing stabilization of the system. These interactions are observed as an increase in electron density in C—C antibonding orbitals that weakens the respective bonds. The electron density at three conjugate π bonds (∼1.63–1.66e) and π* bonds (∼0.32–0.46e) of the molecule clearly demonstrates strong delocalization leading to stabilization of energy in the range 16.51–24.82 kcal/mol.

The intramolecular hyperconjugative interaction of π electrons from (C4—C5) distribute to π*(C2—C3) and π*(C6—C7) leading to high stabilization energies of 20.47 and 24.82 kcal/mol. These enhanced NBOs further conjugate with antibonding orbitals of π*(C4—C5) and π*(C2—C3), π*(C4—C5) respectively. This results in an enormous stabilization of 208.39, 261.82 and 122.72 kcal/mol, respectively.

An important interaction, related to the resonance in the molecule is the electron donation from nitrogen atom n1(N9) to σ*(C7—C8) leading to moderate stabilization energy of 11.14 kcal/mol, while both the chlorine atoms n3(Cl 1) and n3(Cl 13) share the energies of 14.33 and 15.34 kcal/mol to π*(C2—C3) and π*(C6—C7) bonds respectively. The same trend is observed in the entire part of the ring as shown in Table 2.

The nature and strength of the intra- and intermolecular hydrogen bonding can be explored by studying the changes in electron densities in vicinity of hydrogen bonds. The NBO approach consists of considering this interaction as an electron transfer from the donor to the acceptor. The C—H···N hydrogen bond, in NBO terms, corresponds to the nitrogen lone pair [n(1) N9] electron transfer to the antibonding σ*(C16—H23) and σ*(C44—H49) orbitals. The energy values corresponding to the charge transfer in the supramolecular complex formed by hydrogen bonding are lower than those estimated for the intramolecular hyperconjugative interactions. Apparently besides charge transfer, other components, such as dipole–dipole interactions, contribute significantly to hydrogen bonding.

It becomes evident from Table 2, hyperconjugation between chlorine lone electron pairs [n(2)Cl 14 and n(2)Cl (50)] and antibonding orbitals [σ*(C6—Cl 13) and σ*(Cl 1—C2)] leads to formation of Cl···Cl bond with the stabilization energy of 0.17 kcal/mol.

The intensities of n(1)N9 with σ*(C16—H23) of unit 2 and with σ*(C44—H49) of unit 4 (0.17 and 0.16 kcal/mol respectively) are comparable with the intensities of n(2) Cl 14 with σ*(C6—Cl 13) (0.17 kcal/mol) and n(2) Cl 50 with σ*(Cl 1—C2) (0.17 kcal/mol). This implies that the strengths of both intermolecular interactions C—N···H and Cl···Cl are of the same order.

A hyperconjugative interaction is found between both the lone pairs on chlorine atom of one sub molecule as donor and the C-H antibond of other sub molecule as acceptor providing a charge transfer from the former moieties to the latter one. This

Table 2
Second order perturbation theory analysis of Fock matrix in NBO basis of 2,6-DCBN tetramer A.

Donor NBO (i)	ED[a](i)/e	Acceptor NBO(j)	ED[a](j)/e	$E^{(2)b}$ (kcal mol^{-1})	ε(j)–ε(i)[c] (a.u.)	F(i,j)[d] (a.u.)
Within unit 1						
π(C2—C3)	1.66690	π*(C4—C5)	0.31680	19.94	0.30	0.069
		π*(C6—C7)	0.46599	18.83	0.27	0.066
π(C4—C5)	1.63593	π*(C2—C3)	0.36616	20.47	0.27	0.066
		π*(C6—C7)	0.46599	24.82	0.26	0.073
π(C6—C7)	1.66883	π*(C2—C3)	0.36616	19.52	0.29	0.068
		π*(C4—C5)	0.31680	16.51	0.30	0.064
σ(C7—C8)	1.97823	σ*(C8—N9)	0.01077	8.09	1.66	0.104
σ(C8—N9)	1.99381	σ*(C7—C8)	0.03132	7.15	1.55	0.094
n(2)Cl 1	1.96327	σ*(C2—C7)	0.04216	5.50	0.81	0.060
n(3)Cl 1	1.91000	π*(C2—C3)	0.36616	14.33	0.32	0.065
n(1) N 9	1.96928	σ*(C7—C8)	0.03132	11.14	1.01	0.095
n (2)Cl 13	1.96327	σ*(C6—C7)	0.04217	5.50	0.81	0.060
n (3)Cl 13	1.91000	π*(C6—C7)	0.46599	15.34	0.31	0.068
π*(C2—C3)	0.36616	π*(C4—C5)	0.31680	208.39	0.01	0.084
π*(C6—C7)	0.46599	π*(C2—C3)	0.36616	261.82	0.01	0.080
		π*(C4—C5)	0.31680	122.72	0.03	0.082
From unit 1 to unit 2						
π(C8—N9)	1.98564	σ*(C16—H23)	0.01549	0.21	0.81	0.012
n (1)N9	1.96928	σ*(C16—H23)	0.01549	0.17	0.97	0.012
n (1)Cl 13	1.99149	σ*(C16—H23)	0.01549	0.09	1.40	0.010
n (2)Cl 13	1.96327	σ*(C16—H23)	0.01549	0.21	0.78	0.012
From unit 1 to unit 3						
None above threshold						
From unit 1 to unit 4						
π(C8—N9)	1.98564	σ*(C44—H49)	0.01498	0.21	0.81	0.012
n (1)Cl 1	1.99149	σ*(C44—H 49)	0.01498	0.09	1.40	0.010
n (2)Cl 1	1.96327	σ*(C44—H49)	0.01498	0.21	0.78	0.012
n (1) N 9	1.96928	σ*(C44—H49)	0.01498	0.16	0.98	0.011
From unit 2 to unit 1						
σ(C16—H23)	1.97700	π*(C8—N9)	0.01830	0.07	0.61	0.006
n(2)Cl 14	1.96441	σ*(C6—Cl 13)	0.02752	0.17	0.45	0.008
From unit 3 to unit 1						
None above threshold						
From unit 4 to unit 1						
σ(C44—H49)	1.97640	π*(C8—N9)	0.01830	0.07	0.61	0.006
n(2)Cl 50	1.96441	σ*(Cl 1—C2)	0.02752	0.17	0.45	0.008

mechanism can explain relatively high occupancies of σ*(C16—H23) and σ*(C44—H49) antibonding orbitals, as shown in Table 2. A gain of occupancy in antibonding acceptor orbitals can be directly correlated with a weakening of the bond associated with this orbital which leads to its elongation and concomitant red-shift of the C—H stretching wavenumber.

According to the data of Table 2, the hyperconjugative interaction of π electrons from (C8—N9) distribute to σ*(C16—H23) and σ*(C44—H49) leading to equal stabilization energy of 0.21 kcal/mol.

Molecular electrostatic potential

The potential applications of the molecular electrostatic potential (MEP) for interpretation and prediction of chemical reactivity have long been recognized. MEP is a rigorously defined physically observable quantity and can be reliably used to elucidate molecular behavior and phenomena in different contexts. The MEP has been applied since its definition to a wide range of fields, such as the study of biological interactions, analysis of molecular similarity, description of the crystalline state, salvation phenomena, and the topographical analysis of the electronic structure of complex molecules [38]. It is typically visualized through mapping its value onto the molecular electron density isosurface. The different values of the electrostatic potential at the surface are represented by different colors. The more the red/blue difference, the more polar is the molecule. The initial tendency of an approaching positive point charge is to go to those regions where the electrostatic potential is the most negative. Hence, in principle, the minima of the MEP map will coincide with the sites of preferred electrophilic attack to the system under investigation. The maxima of the MEP are located only at the nuclei and offer information on the preferred sites for nucleophilic substitutions. Fig. S2 shows the 3D electrostatic potential contour map. MEP plot shows that the negative region (red color) is associated with the nitrogen atom of the cyano (C≡N) group, showing most favorable site for electrophilic attack. When focused on positive regions of the electrostatic potential, we found that the hydrogen atoms of the phenyl ring are surrounded by blue color, indicating that these sites are probably involved in nucleophilic processes. The chlorine atoms seem to be exerting almost neutral electrostatic potential (green color).

Thermal analysis

Differential scanning calorimetry (DSC) has been performed in order to check the purity of the sample. The DSC trace (Fig. 1) indicates a sharp endotherm starting at 144.20 °C which coincides very well with the melting point of the sample [39]. The heat of fusion is −65.34 J/g. No thermal-induced glass transition and crystallization is observed during the course of heating, hence the compound is thermally stable.

NMR analysis

NMR is a sensitive and versatile probe of molecular-scale structure and dynamics in solids and liquids. It enables to get faster and

Table 3
Experimental and theoretical chemical shifts (ppm) of 2,6-DCBN in ^{13}C NMR spectra.

Atom number	Cal.	Exp.
C6	154.49	138.62
C2	154.49	138.62
C4	135.91	136.00
C5	131.87	129.60
C3	131.87	129.60
C7	119.65	114.65
C8	116.61	114.00

easier structural information. After optimization, ^{13}C NMR shieldings were calculated using the GIAO method [40,41] at B3LYP/6-311++G(d,p) level. Absolute isotropic magnetic shieldings were transformed into chemical shifts by referencing to the shielding of a standard compound tetramethylsilane (TMS), computed at the same theoretical level.

$$\delta_x^{rel} = \delta_{TMS}^{abs} - \delta_x^{abs} \quad (3)$$

The theoretical ^{13}C chemical shifts have been compared with experimental data (Table 3), and are found to be in compliance with experimental findings. The chemical shifts of the carbons of the phenyl ring have been calculated in a broad range 116.61–154.49 ppm due to substitution on the phenyl ring. The carbons with which the chlorine atoms are attached are the most downfield (δ = 154.49 ppm). This is due to the reason that chlorine is an electron withdrawing group; hence it reduces the electron density on C2 and C6 atoms. This causes less shielding at C2 and C6 atoms which increases the chemical shifts on these carbons. The cyano group attached to C1 atom is a moderate electron withdrawing group, so C1 atom has absorption at a lower value (δ = 119.65 ppm). There is a difference in the calculated and experimental values of the chemical shifts of the carbon atoms attached to chlorine atoms and cyano group. This may be due to the susceptibility of the chemical shifts to intermolecular interactions which affects the structure and orientation of the molecules. Theoretical calculations are usually performed at vacuo and NMR measurements in solution, in which the solvation as well as other thermodynamic equilibria play crucial roles influencing the values of the chemical shifts.

Vibrational analysis

The harmonic vibrational wavenumbers of 2,6-DCBN have been computed in the isolated state and in the tetramer form at B3LYP/6-311++G(d,p) level. Four wavenumbers appear for each vibration corresponding to the four molecules in the tetramer. The computed wavenumbers, the corresponding experimental FTIR and FT-Raman wavenumbers together with respective potential energy distribution (PED) and mode assignments are collected in Table 4. The experimental FT-IR spectra in the region 4000–400 cm^{-1} and the FT-Raman spectra in the region 4000–200 cm^{-1} along with theoretically simulated monomer and tetramer spectra are given in Figs. 6 and 7, respectively.

C—H stretching vibrations

The aromatic C—H stretching bands are observed at 3091 cm^{-1} in the FTIR and at 3094, 3067 cm^{-1} in the FT-Raman spectra. As seen, these bands are not affected appreciably by the nature of substituents. In compounds, 4-hydroxy benzonitrile, 4-chloro-3-nitrobenzonitrile and in p-fluoro benzonitrile [42–44] having different substituents, the C-H stretching bands have been observed in the same range as in 2,6-DCBN. In the IR spectra, the C—H stretching bands are found to be weak. This may be due to a decrease in the dipole moment caused by the reduction of negative charge on the carbon atom. This reduction occurs because of the electron substituent on the carbon atom by the substituent. The scaled wavenumbers calculated by B3LYP/6-311++G(d,p) are at 3072, 3068 and 3047 cm^{-1} in the isolated state. In the simulation with tetramer form, the C—H stretching modes corresponding to two units show a blue shift of 9, 6 and 15 wavenumbers [Fig. 8(a)], as out of four, C—H groups of two units are involved in intermolecular hydrogen bonding. The DFT calculations exhibit that the intensities of two of these modes in tetramer are about 33 and 2 times than that of monomer while the center peak is of negligible intensity.

The C—H bending vibrations usually occur in the frequency region 1500–1250 cm^{-1} [45]. The bands observed at 1431, 1271 and 1198 cm^{-1} in the FTIR spectra and at 1432, 1272 and 1208 cm^{-1} in the FT-Raman spectra in 2,6-DCBN with strong to medium intensities have been assigned to C—H in plane bendings. These vibrations have been calculated at 1439, 1437, 1208 and 1170 cm^{-1} and show a good match with the experimental values. These modes are coupled with phenyl ring C—C stretching vibrations. The position of C—H deformation is determined almost extensively by the relative position of the substituents and is independent of nature [46]. The bands observed at 1260, 1145, 1095 cm^{-1} in 3,5-dichlorobenzonitrile [47] and at 1265, 1100 cm^{-1} in 2,4-dichlorobenzonitrile [48] in the FTIR spectra support this statement.

The C—H out-of-plane bending vibrations occur in the frequency range 1000–675 cm^{-1} [49]. These bending vibrations are predicted theoretically at 989, 905 and 788 cm^{-1}. In the tetramer simulation, these values shift slightly towards higher wavenumbers at 1002 and 921 cm^{-1} while the 788 cm^{-1} band remains almost unchanged. Gauss view results indicate that the mode which is unaffected is due to C—H belonging to units 1 and 3, which are not involved in hydrogen bonding. No evidence was found for the existence of $n(N9) \rightarrow \sigma^*(C17—H24)$ and $n(N9) \rightarrow \sigma^*(C45—H48)$ hydrogen bonds on the grounds of NBO interactions.

C—C vibrations

The ring C—C stretching vibrations are of variable intensity and give rise to characteristic bands in both the IR and the Raman spectra, covering the spectral range from 1600–1400 cm^{-1} [50]. The theoretically scaled C—C stretching vibrations by DFT method at 1587, 1563, 1439, 1437, 1284, 1211, 1170 and 1077 cm^{-1} show a good agreement with the recorded FT-IR and FT-Raman spectral data as shown in Table 4. The PED corresponding to all C—C stretching vibrations lies between 35% and 92% in combination with C—H in-plane bending and ring deformations. This is consistent with the literature data [42,51,52]. The ring in-plane vibrations have given rise to weak bands in the wavenumber region, below 1100 cm^{-1}. The trigonal ring deformation modes have been calculated at 1103, 1077 and 777 cm^{-1}. Two of these modes show a large shifting of wavenumbers in the tetramer form. These modes are affected in magnitudes upon substitution. The ring puckering and torsion modes have been observed below 800 cm^{-1} as highly coupled modes.

C≡N group vibrations

The C≡N stretching mode can be used as a good probe for evaluating the bonding configuration around the cyano nitrogen atom and the electronic distribution on the phenyl ring. The n–π conjugation between the cyano nitrogen lone electron pair and the phenyl ring is strong in the ground state. The C≡N stretching mode appears as a single, normally intense absorption in the range 2240–2200 cm^{-1} in different benzonitrile derivatives [53–55,47,56]. The geometry of the cyano group is affected insignificantly by new substituents on the phenyl ring. Hence, the vibrational wavenumbers of the cyano group does not change much from the benzonitrile molecule, in which, this band has been

Table 4
Experimental and calculated wavenumbers of 2,6-DCBN monomer and tetramer A and their assignments.

Cal. wavenumbers (cm^{-1}) monomer		Cal. wavenumbers (scaled) (cm^{-1}) Tetramer A	Expt. freq. (cm^{-1})		[a]Assignments (% PED)
Unscaled	Scaled		IR	Raman	
3212	3072	3081, 3081, 3078, 3078	3091	3094	ν(C5—H12)(43) + ν(C3—H10)(42) + ν(C4—H11)(14)
3208	3068	3074, 3074, 3071, 3071		3067	ν(C3-10)(50) + ν(C5—H12)(49)
3185	3047	3062, 3062, 3050, 3050			ν(C4—H11)(85) + ν(C5—H12)(7) + ν(C3—H10)(7)
2342	2273	2271, 2271, 2267, 2267	2233	2234	ν(C8—N9)(88) + ν(C7—C8)(12)
1615	1587	1588, 1587, 1587, 1586	1571		ν(C—C)(Ring)(70) + δasym(Ring)(10) + δ(C5—H12)(7) + δ(C3—H10)(7)
1590	1563	1563, 1563, 1561, 1560	1558	1559	ν(C—C)(Ring)(70) + δ(C4—H11)(15) + δ'_{asym}(Ring)(9)
1461	1439	1440, 1440, 1437, 1437	1431	1443	ν(C—C)(Ring)(35) + δ(C4—H11)(24) + δ(C5—H12)(16) + δ(C3—H10)(16)
1459	1437	1436, 1436, 1435, 1435			ν(C—C)(Ring)(39) + ν(C7—C8)(17) + δ(C3—H10)(16) + δ(C5—H12)(16)
1300	1284	1286, 1286, 1286, 1286	1271	1272	ν(C—C)(Ring)(92)
1225	1211	1212, 1211, 1211, 1211	1198	1208	ν(C7—C8)(31) + ν(C—C)(Ring)(24) + δ(C3—H10)(12) + δ(C5—H12)(12) + $\delta_{trigonal}$(Ring)(7)
1222	1208	1209, 1209, 1206, 1206			δ(C5—H12)(24) + δ(C3—H10)(24) + ν(C—C)(Ring)(30) + δ(C7—C8)(7)
1183	1170	1172, 1172, 1166, 1161		1179	δ(C4—H11)(54) + ν(C—C)(Ring)(20) + δ(C3—H10)(6) + δ(C5—H12)(6)
1114	1103	1104, 1103, 1097, 1096	1108	1113	$\delta_{trigonal}$(Ring)(44) + ν(C2—Cl 1)(16) + ν(C6—Cl 13)(16)
1087	1077	1078, 1078, 1077, 1077	1098	1063	ν(C—C)(Ring)(50) + $\delta_{trigonal}$(Ring)(15) + δ(C3—H10)(12) + δ(C5—H12)(12)
997	989	1002, 1000, 990, 990	982		δ_{oop}(C4—H11)(53) + δ_{oop}(C5—H12)(17) + δ_{oop}(C3—H10)(17) + $\tau_{puckering}$(Ring)(9)
911	905	921, 921, 906, 906	907		δ_{oop}(C3—H10)(45) + δ_{oop}(C5—H12)(45) + τ'_{asym}(Ring)(7)
799	796	801, 797, 796, 795	800		δ'_{asym}(Ring)(35) + ν(C6—Cl 13)(27) + ν(C2—Cl 1)(27)
791	788	790, 789, 788, 788	782	780	δ_{oop}(C5—H12)(25) + δ_{oop}(C3—H10)(25) + δ_{oop}(C4—H11)(19) + $\tau_{puckering}$(Ring)(18) + δoop(C6—Cl 13)(5) + δoop(C2—Cl 1)(5)
790	777	786, 786, 785, 784			δ_{asym}(Ring)(35) + $\delta_{trigonal}$(Ring)(24) + ν(C7—C8)(19) + ν(C—C)(Ring)(6) + ν(C—C)(Ring)(6)
741	738	732, 732, 728, 728	715	718	$\tau_{puckering}$(Ring)(51) + δoop(C7—C8)(18) + δoop(C2—Cl 1)(9) + δoop(C6—Cl 13)(9) + δoop(C4—H11)(7)
605	604	607, 607, 604, 604	619		δ(C7—C8)(41) + δ(C7—C8—N9)(23) + δ'_{asym}(Ring)(9) + δ(C2—Cl 1)(5)+ δ(C6—Cl13)(5) + ν(C—C)(Ring)(10)
583	583	579, 579, 579, 579			$\tau_{puckering}$(Ring)(32) + τ_{asym}(Ring)(24) + τ(C7—C8)(16) + δoop(C7—C8) (15) + δoop(C4—H11)(7)
550	550	551, 551, 549, 548	547	552	ν(C7—C8)(20) + δ_{asym}(Ring)(19) + ν(C2—Cl 1)(14) + ν(C6—Cl 13)(14) + ν(C—C)(Ring)(12)
542	542	546, 545, 542, 542			τ'_{asym}(Ring)(43) + δ_{oop}(C2—Cl 1)(28) + δ_{oop}(C6—Cl 13)(28)
424	425	429, 429, 426, 426	426	413	δ'_{asym}(Ring)(49) + ν (C2—Cl 1)(16) + ν(C6—Cl 13)(16) + δ(C7—C8—N9)(8)
421	422	425, 425, 424, 424			τ_{asym}(Ring)(46) + τ(C7—C8)(21) + δ_{oop}(C6—Cl 13)(10) + δ_{oop}(C2—Cl 1)(10)
362	363	364, 364, 362, 362	402	365	δ_{asym}(Ring)(40) + ν(C6—Cl 13)(19) + ν(C2—Cl 1)(19) + $\delta_{trigonal}$(Ring)(9) + ν(C7—C8)(5)
359	360	361, 361, 359, 359	–		δ(C6—Cl 13)(37) + δ(C2—Cl 1)(37) + δ(C7—C8—N9)(20)
203	204	209, 209, 206, 206	–	209	δ_{oop}(C7—C8)(40) + δ_{oop}(C2—Cl 1)(19) + δ_{oop}(C6—Cl 13)(19) + τ(C7—C8)(14)
201	202	206, 205, 204, 204	–		δ(C6—Cl 13)(42) + δ(C2—Cl 1)(42) + δ_{asym}(Ring)(6)
198	199	203, 203, 202, 201	–		τ'_{asym}(Ring)(72) + δoop(C5—H12)(8) + δoop(C3—H10)(8) + δoop(C6—Cl 13)(7) + δoop(C2—Cl 1)(7)
139	140	148, 146, 142, 142	–	–	δ(C7—C8)(48) + δ(C7—C8—N9)(40) + τ(C7—C8)(5)
79	80	88, 85, 82, 81	–	–	τ_{asymm} (Ring)(54) + τ(C7—C8)(14) + $\tau_{puckering}$(Ring)(13) + δ_{oop}(C7—C8)(8)

[a] *Types of vibration:* ν, stretching; δ, deformation; oop, out of plane bending; in, in plane bending; τ, torsion; tri, trigonal; asym, asymmetric.

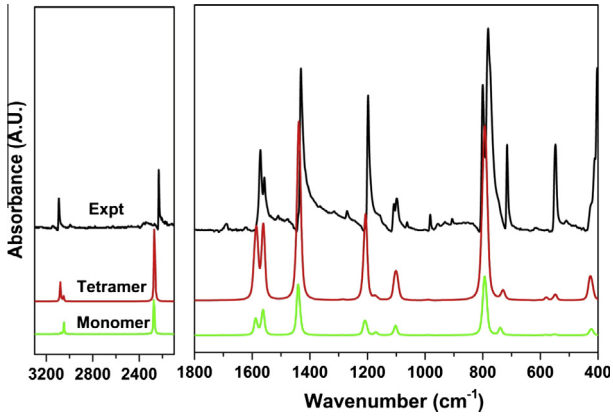

Fig. 6. Comparison of FT-IR spectra with theoretically scaled monomer and tetramer spectra of 2,6-DCBN.

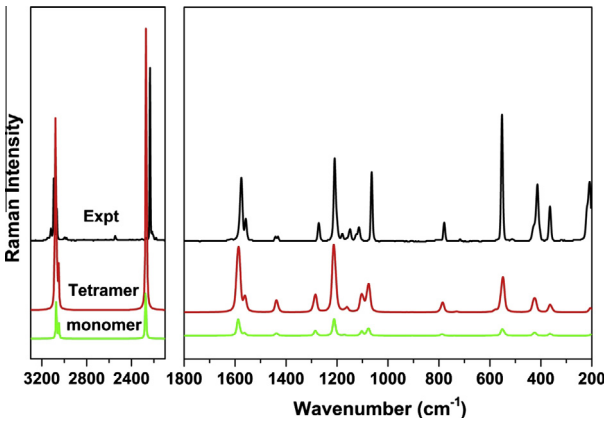

Fig. 7. Comparison of FT-Raman spectra with theoretically scaled monomer and tetramer spectra of 2,6-DCBN.

identified at 2230 cm^{-1} [35]. The IR intensity, which varies from medium to strong, depends on the substituent. Electron withdrawing groups such as —F, —Cl, —Br, —NO_2, —OH, or —CF_3, decrease the IR band intensity and increase the wavenumber value to the higher limit of the characteristic spectral region, whereas the electron donating groups, such as —NH_2 increase the IR intensity and decrease the wavenumber value [57]. As in 4-hydroxybenzonitrile [42], in 4-chloro-3-nitroenzonitrile [43] and in p-fluorobenzonitrile [44], the electron withdrawing groups (—OH, —Cl and —F, respectively) increase the wavenumber to 2234 cm^{-1}, 2238 cm^{-1} and 2238 cm^{-1} in the FTIR spectra. The electron donating groups such as 2-amino-4-methyl-benzonitrile [54] reduces the —C≡N

stretching vibration to 2211 cm^{-1} in FTIR spectra. In 2,6-DCBN it is observed at 2233 cm^{-1} in the FT-IR spectra. The stretching mode is highly localized on the C≡N bond with a total energy distribution of 88%. It is mixed with C—C stretching to the extent of 12%. In 2,6-DCBN it is observed at 2233 cm^{-1} in the FT-IR spectrum and at 2234 cm^{-1} in FT-Raman spectrum. The stretching mode is highly localized on the C≡N bond with a total energy distribution of 88%. It is mixed with C—C stretching to the extent of 12%. In the present case, the electron withdrawing group (—Cl) slightly decreases the FT-IR band intensity. The Raman intensity of the C≡N band is enhanced by the conjugation of the aromatic ring.

In the isolated state, the scaled value at 2273 cm^{-1} corresponds to the C≡N stretching mode. The difference in the scaled and experimental values may be due to the involvement of cyano group in the hydrogen bond. The wavenumber of this mode is affected little in the tetramer simulation and gets closer to the experimental value [Fig. 8(b)]. The intensity of ν (C≡N) band of tetramer A is about seven times higher than that of monomer.

In plane and out of plane bending modes of C≡N group also appear with weak IR intensity and strong Raman activity. There are different modes to which the δ (C≡N) bending vibrations contribute significantly. The C≡N in plane bending vibrations have been predicted theoretically at 604, 360 and 140 cm^{-1} and are observed at 619, 402 cm^{-1} in FT-IR spectra; and at 365, 209 cm^{-1} in FT-Raman spectra. A peak at 209 cm^{-1} in the FT-Raman spectra has been attributed to C≡N out of plane bending. The scaled value at 204 cm^{-1} corresponds to this peak. This mode is highly coupled with C—Cl out of plane bending vibrations. The (C—CN) in plane and out of plane bending vibrations have been calculated at 604, 140; and 583 cm^{-1} respectively. A slight deviation appears between the scaled wavenumbers of the isolated state and the simulated tetramer of these modes which improve the spectra but the calculated hydrogen bonds are too weak.

C—Cl vibrations

The C—X (X = Cl, F, Br, I) group generally gives strong bands in the frequency range of 1130–480 cm^{-1} [58]. The position of the bands is influenced by neighboring atoms or groups – the smaller the halide atom, the greater the influence of the neighbor. Bands of weak to medium intensity are also observed due to overtones of the C—X stretching vibrations.

In general, the C—Cl stretching spreads out between two or more normal modes [59,60]. In 2,6-DCBN, the C—Cl stretching has been observed in the range 1100–400 cm^{-1}. It has been observed that in mono chloro benzene derivatives, such as in 4-chloro-3-nitro benzonitrile [43], 2-amino-5-chlorobenzonitrile [55], the C—Cl stretching frequency appears in 600–800 cm^{-1} region, whereas in dichloro benzene derivatives, as 2-amino-3, 5-dichlorobenzonitrile [53], the C—Cl stretching is observed in the range 1100–400 cm^{-1}. In present investigation, the strong bands observed at 1108, 800, 547 and 402 cm^{-1} in FTIR spectra have been assigned to C—Cl stretching vibrations. When a halogen atom is attached directly to the ring, the C—X stretch vibrations tend to interact with the ring vibrations [61]. As revealed by PED, the C—Cl vibrations are strongly coupled with ring asymmetric bending and C—C stretching vibrations. The tetramer simulated values of these modes at 1096, 801, 548 and 364 cm^{-1} are close to the experimental ones. The C—Cl in-plane and out-of-plane bending vibrations are expected in the low wavenumber region. The C—Cl in plane bending modes have been calculated at 360, 202 cm^{-1} and out of plane bending modes at 738, 542, 422 and 204 cm^{-1}. These values give a good match to the experimental data. The out of plane bending modes are strongly coupled with ring torsion modes. The simulated tetramer wavenumbers having contribution from C—Cl out of plane bending shows a shifting of 10, 4, 3 and 5 wavenumbers as compared to the monomer [Fig. 8(c) and (d)].

In condensed-phase molecular systems, intermolecular interactions induce a large variety of spectral manifestations. In fact, it is commonly observed that the gas-to-condensed phase transition leads to variations of the observables of a spectral band, such as band intensities and shapes, frequency position of band maxima. These spectral variations are determined by the nature and the efficiencies of the perturbations of the energy levels involved in each spectral band, which in turn depend on the molecular nature of the condensed-phase system.

It is seen that the wavenumber shifts in the modes on going from monomer to tetramer due to each of the CN···H and Cl···Cl interactions is of the same order; hence these interactions are comparable in energy. The magnitude of interaction and hence the observables of the spectral band depend on the functional and the basis set used. This is exhibited nicely in Fig. S3; where the simulated IR and Raman spectra due to various functionals and basis sets B3LYP/6-31G, M062X/6-31G, HF/6-31G and HF/3-21G have been shown for 2,6-DCBN in the isolated state and in the tetramer form. It is observed from the simulated spectra that the wavenumber shifts are present in a large number of modes and in large magnitude for M062X/6-31G and HF/3-21G whereas few modes are affected for B3LYP/6-31G and HF/6-31G. However the changes in line shape and intensity are seen for the latter as well as the former ones.

Interaction energy calculations

For a supermolecule ABCD, made up of four interacting systems A, B, C and D, the interaction energy can be expressed as the energy difference between the whole system and its subunits, each evaluated at their own geometries in their own basis sets

$$\Delta E_{unc}(ABCD) = E_{ABCD}(ABCD) - E_A(A) - E_B(B) - E_C(C) - E_D(D) \quad (4)$$

However, the use of finite basis sets centered on the nuclei and, in essence, the linear combination of atomic orbitals–molecular orbitals (LCAO–MO) formalism, leads to the basis set superposition error (BSSE). The main consequence is that the interaction energy is artificially overestimated. However, effects on the molecular geometry or on the electronic density can be important and should be taken into account. To compute the correct value of the interaction energy, we need to use (nearly) complete basis sets on the supermolecule and on each subunit, which is usually impossible in practice. The most widely used way to handle BSSE has been the full counterpoise method [62] which is based on the assumption that the error is minimized if the same basis set is used for the description of both the supermolecule and its fragments.

In the counterpoise scheme, the interaction energy $\Delta E_{CP}(ABCD)$ is defined as the difference of the energies of the supermolecule and the subnits, all computed in the same supermolecule basis set:

$$\Delta E_{CP}(ABCD) = E_{ABCD}(ABCD) - E_A(ABCD) - E_B(ABCD) - E_C(ABCD) - E_D(ABCD) \quad (5)$$

Eqs. (4) and (5) will converge when a complete basis set is used. One can define the BSSE content in the interaction energy as

$$\delta E(BSSE) = \Delta E_{unc}(ABCD) - \Delta E_{CP}(ABCD) = E_A(ABCD) - E_A(A) + E_B(ABCD) - E_B(B) + E_C(ABCD) - E_C(C) + E_D(ABCD) - E_D(D) \quad (6)$$

The interaction energy of 2,6-DCBN tetramer was estimated and the effect of basis set superposition error (BSSE) was analyzed for understanding the nature of the hydrogen bond. BSSE is considered to be one of the major sources of error in the calculation of the interaction energy of weakly bound (Van der Waals) systems. Many papers have indicated that the impact of BSSE on weakly bound

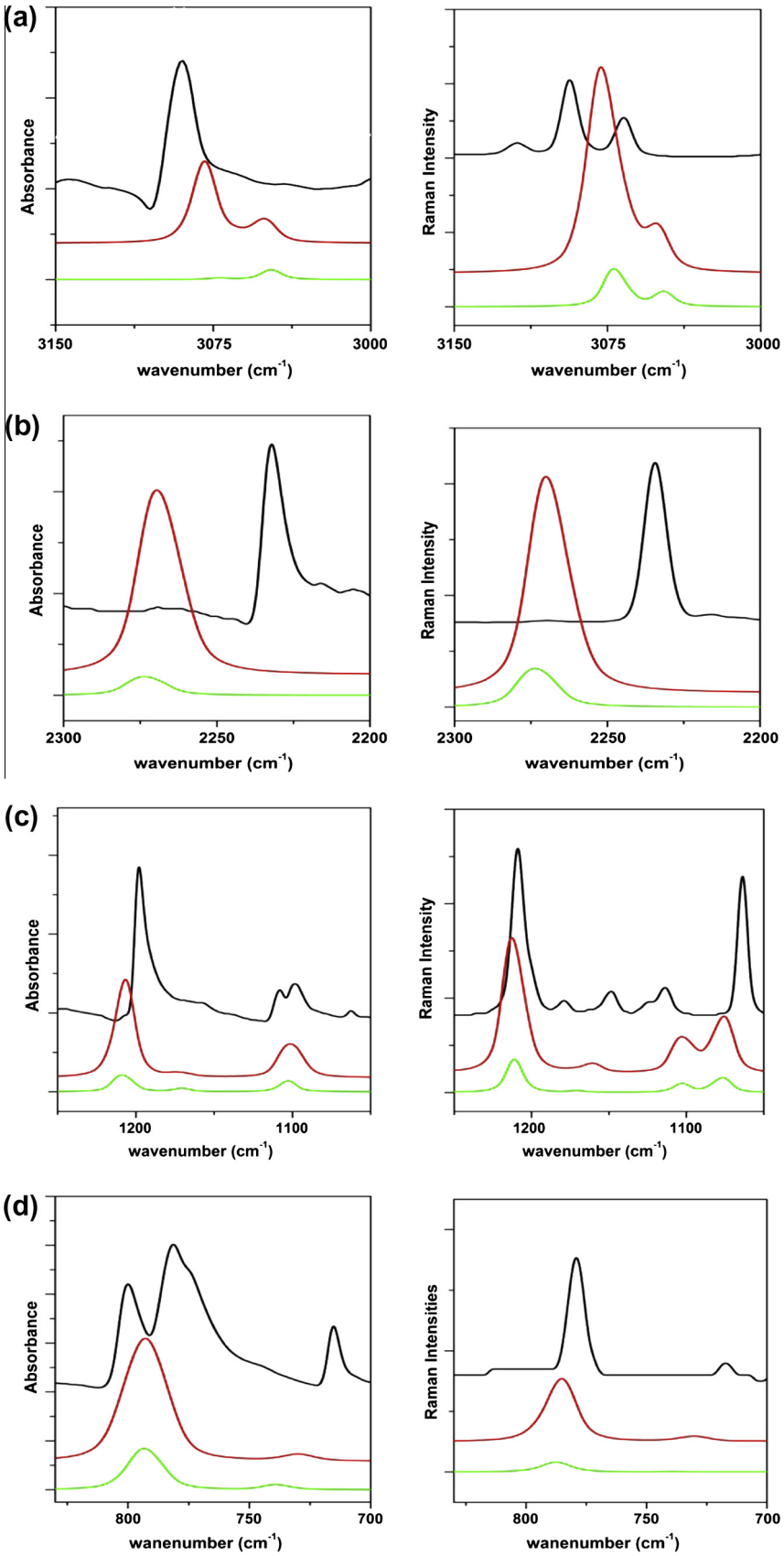

Fig. 8. Theoretically scaled Infrared and Raman spectra of monomer and tetramer simulations along with experimental ones. Green, red and black represent monomer, tetramer and experimental spectra, respectively. (For interpretation of the references to color in this figure legend, the reader is referred to the web version of this article.)

Table 5
Calculated intermolecular interaction energy of 2,6-DCBN tetramer A for different functionals and basis sets.

Functional	ΔE with BSSE (kcal/mol)	ΔE without BSSE (kcal/mol)	BSSE (kcal/mol)
HF/3-21G	−5.22425	−15.0043	9.78005
HF/6-31G	−5.17978	−8.20275	3.02297
HF/6-311++G(d,p)	−4.88241	−7.31502	2.43261
B3LYP/6-31G	−6.8189	−10.9653	4.1464
M062X/6-31G	−13.5577	−17.9175	4.3598

systems is smaller for the DFT method than that for ab initio methods such as the HF, but its influence even in case of DFT could not be neglected [63]. To confirm the reliability of calculated results, DFT with hybrid B3LYP functional and HF methods were chosen and the effect was estimated using basis set 6-31G. The corresponding interaction energies, uncorrected and corrected for the BSSE together with the BSSE are listed in Table 5. As reflected from Table 5, the corrected interaction energy of 2,6-DCBN tetramer is lower for DFT with hybrid B3LYP functional, than for HF using 6-31G basis set. The magnitude indicates that the interaction between subunits is weak.

To determine the appropriateness of the chosen functional B3LYP for the calculations, we have also determined the interaction energy for M062X functional that gives an excellent accuracy in describing weakly interacting, dispersions dominated systems (errors of ∼0.25 kcal/mol) [64]. The difference in the values of the interaction energy (ΔE) with BSSE by using two functionals is 6.739 kcal mol^{-1}, lower being for B3LYP functional.

The obtained interaction energy values corrected for the BSSE were further checked for the use of finite basis sets in the optimization procedure. The basis set size plays a major role due to the intermolecular BSSE. The BSSE corrected energies of the tetramer for HF with 3-21G, 6-31G and 6-311++G(d,p) are 9.780, 3.023 and 2.433 kcal/mol; respectively, accounting for 65.2%, 36.85% and 33.26% of the interaction energy before BSSE correction, The difference in the counterpoise corrected and uncorrected interaction energies, which indicate the magnitude of BSSE due to the basis set superposition decreases with the increase in the size of the basis set, as essentially the BSSE should disappear as the basis set limit is reached. This shows that the BSSE correction is important, mostly in case of smaller basis set.

The intermolecular interactions could significantly influence the normal mode vibrations, resulting in red shift or improper blue shifting [65] of the vibrational wavenumbers. The normal mode vibrations depend very much on the applied method or basis set, and last but not the least on the BSSE effects [63]. It should be mentioned that BSSE is not a real physical effect and normally it must be considered together with the intermolecular effects. However to see how important wavenumber shifts could be induced by the BSSE, harmonic vibrational wavenumbers have been calculated for the non corrected and corrected BSSE potential energy surface (PES). Table S3 summarizes the results for the tetramer together with the monomer. As the BSSE correction to the interaction energy is small in HF/6-31G and B3LYP/6-31G, the wavenumber shifts are observed only in few modes mainly in intermolecular modes. On visualizating their vibrational character by Gauss view, we find that major changes are found in modes having contribution of C-H out of plane bending (mode no. 16, 18). Mode no. 13 consisting of ring deformation and C—Cl stretching vibrations underwent a shifting of 15 wavenumbers. A difference of about 10–15% was found in the wavenumbers of intermolecular modes. However calculations with HF/3-21G and M062X/6-31G reveal wavenumber shifts in a number of modes on the BSSE-counterpoise corrected PES.

The aforementioned analysis shows that counterpoise wavenumbers at the B3LYP level with higher basis sets are not much different as compared with the wavenumbers obtained without employing the counterpoise correction scheme in the optimization. Present vibrational study is based on calculations at DFT/B3LYP level using 6-311++G(d,p) basis set.

UV–vis spectral analysis

The UV–vis absorption spectrum of the sample in methanol solvent, is shown in Fig. 2. The ground state fully optimized geometry was used to evaluate the excitation energies and oscillator strengths of the electronic excitations of 2,6-DCBN using time-dependent density functional theory (TD-DFT) [66,67] method with solvent effect modeled by polarizable continuum model (PCM) [68,69]. TD-DFT is the natural extension of ordinary density functional theory to the time domain which grants access to its excited state and non-equilibrium properties. In TD-DFT, the complicated many-body time-dependent Schrödinger equation is replaced by a set of time dependent single-particle equations whose orbitals yield the same time-dependent density $n(\mathbf{r},t)$. As can be seen from the UV–vis spectra (Fig. 2), absorption maxima are found at 286.4, 234.1 and 215.3 nm. The calculated results involving the vertical excitation energies, oscillator strengths and wavelengths along with the experimental wavelengths are presented in Table 6. A close agreement has been obtained between the experimental and the calculated values of wavelengths. The lowest energy transition corresponds to HOMO → LUMO configuration. However the oscillator strength is very weak. The features of the HOMO and LUMO of the title molecule with energy values

Table 6
Calculated absorption wavelengths, energies and oscillator strengths of 2,6-DCBN using TD-DFT method.

Transition type	λ (nm)		Transition energy *E*(ev)	Oscillator strength (f)	Assignment
	Exp.	Cal.			
Gas phase					
H → L	–	271.07	4.5739	0.0400	π, π*
H → L + 1	–	213.26	5.8139	0.3001	π, π*
H-1 → L + 1	–	210.07	5.8980	0.4258	π, π*
Methanol					
H → L	286.4	275.76	4.4960	0.0795	π, π*
H → L + 1	234.1	213.30	5.8125	0.3977	π, π*
H-1 → L + 1	215.3	208.55	5.9450	0.4880	π, π*

can be seen in Fig. S4. The HOMO is localized partially on the phenyl ring and on the chlorine atoms, whereas, the LUMO is localized almost on the whole molecule. Molecular orbital coefficients analyses based on optimized geometry indicate that the frontier molecular orbitals HOMO and LUMO are mainly composed of p atomic orbitals. So above electronic transition is mainly derived from the contribution of bands $\pi \rightarrow \pi^*$.

A comparison of the calculations in gas phase and in methanol solvent reveals that the positions of absorption maxima are slightly shifted by solvent effects. It is evident from the table that the calculated absorption band corresponding to lowest excited state has shown a red shift. The reason for this red shift is the solvent effect which can affect the geometry and the electronic structure as well as the properties of the molecule. The highest oscillator strength (0.4880) has been seen in the transition from HOMO−1 to LUMO+1. Another strong transition (oscillator strength 0.3977) is calculated at 213.30 nm and it correlates well to the experimental band at 234.1 nm in methanol.

Quantum chemical calculations are able to provide some general information about the structure of molecules in the excited electronic states. Significant changes are observed in the molecular geometry on electronic excitation due to change in the nature of molecular orbitals. The excited-state hydrogen bonding structure and dynamics have been studied through a comparison of the hydrogen bonded 2,6-DCBN tetramer to the isolated monomer in ground and electronic excited state. The optimized geometries of monomer and tetramer in the first excited state (S_1) have been compared with those in the ground state (S_0) using HF method employing 6-31G basis set and are shown in Table 7. The optimized structures of the monomer and the tetramer in excited state

Table 7
Comparison of geometrical parameters optimized in ground and excited states..

Geometrical parameters	HF/6-31G ground state	HF/6-31G excited state	HF/3-21G ground state	HF/3-21G excited state
Bond length (Å)				
ν(C2—C7)	1.3926	1.4602	1.3854	1.4594
ν(C6—C7)	1.3926	1.4602	1.3853	1.4597
ν(C2—C3)	1.3784	1.3609	1.3721	1.3518
ν(C3—C4)	1.3855	1.4139	1.3825	1.4144
ν(C4—C5)	1.3855	1.4139	1.3821	1.4142
ν(C5—C6)	1.3784	1.3609	1.3725	1.3519
ν(C7—C8)	1.4296	1.3703	1.4229	1.3615
ν(C2—Cl 1)	1.7952	1.7860	1.8014	1.7920
ν(C3—H10)	1.0697	1.0701	1.0688	1.0693
ν(C4—H11)	1.0715	1.0706	1.0705	1.0692
ν(C5—H12)	1.0697	1.0701	1.0689	1.0693
ν(C6—Cl 13)	1.7952	1.7860	1.8012	1.7919
ν(C8—N9)	1.1456	1.1875	1.1385	1.1750
Bond angles (°)				
ø(C3—C2—C7)	121.731	121.793	122.006	122.069
ø(C4—C3—C2)	119.326	120.260	119.236	120.228
ø(C5—C4—C3)	120.381	120.279	120.223	120.142
ø(C6—C5—C4)	119.326	120.260	119.252	120.228
ø(C8—C7—C6)	121.248	122.193	121.330	122.360
ø(C8—C7—C2)	121.248	122.193	121.374	122.373
ø(C3—C2—Cl 1)	118.355	120.286	118.382	120.512
ø(C2—C3—H10)	119.735	119.829	119.694	119.847
ø(C3—C4—H11)	119.809	119.860	119.862	119.924
‘ø(C4—C5—H12)	120.937	119.909	121.102	119.928
ø(C5—C6—Cl 13)	118.355	120.286	118.374	120.519
ø(C7—C8—N9)	180.000	180.000	179.995	179.980
Bond torsions (°)				
t(C4—C3—C2—C7)	0.000	0.000	0.000	0.000
t(C5—C4—C3—C2)	0.000	0.000	0.000	0.000
t(C6—C5—C4—C3)	0.000	0.000	0.000	0.000
t(C8—C7—C6—C5)	180.000	180.000	180.000	180.000
t(C6—C7—C2—Cl 1)	180.000	180.000	180.000	180.000
t(C7—C2—C3—H10)	180.000	180.000	180.000	180.000
t(C2—C3—C4—H11)	180.000	180.000	180.000	180.000
t(C3—C4—C5—H12)	180.000	180.000	180.000	180.000
t(C4—C5—C6—Cl 13)	180.000	180.000	180.000	180.000
t(C5—C6—C7—C8)	180.000	180.000	180.000	180.000
Intermolecular parameters				
Bond length (Å)				
ν(N9···H23)	2.9596	2.9776	2.7915	2.9691
ν(N9···H49)	2.9562	3.1661	2.7893	3.0405
ν(N35···H25)	2.9570	2.9857	2.7914	2.6369
ν(N35···H47)	2.9590	2.7586	2.7920	2.7740
ν(Cl 13···Cl 14)	5.2183	4.5221	3.6293	4.1110
ν(Cl 1···Cl 50)	4.5867	5.1464	3.6342	4.3874
ν(Cl 27···Cl 26)	4.5877	4.7461	3.6350	6.8843
ν(Cl 39···Cl 40)	5.2096	7.2411	3.6304	4.1541
Bond angles (°)				
ø(C8—N9···H23)	109.603	108.979	101.734	99.221
ø(C8—N9···H49)	110.279	104.144	101.655	96.302
ø(C6—Cl 13···C 14)	123.700	155.908	167.912	164.130
ø(C2—Cl 1···Cl 50)	156.869	132.733	167.831	138.552

are shown in Fig. S5(a) and (b) respectively. It is seen from Table 7 that in the excited state, the bond lengths C2—C3, C5—C6, C7—C8 decrease by 0.018, 0.017 Å, 0.059 Å, while C2—C7, C6—C7, C3—C4 and C4—C5 increase by 0.068 Å, 0.068 Å, 0.028 Å, 0.028 Å, respectively, as compared to the ground state. These changes may be due to transfer of π electrons from the region of bonds C2—C7, C6—C7, C3—C4 and C4—C5 to C7—C8 and C4—H11 followed by redistribution of electron charge as shown in HOMO LUMO plot (Fig. 9). The bond lengths C6—Cl 13 and C2—Cl 1 are shorter in the excited state (1.786 Å) than those in the ground state (1.795 Å). This is due to the reduction in the conjugation of chlorine atoms with the neighboring bonds in the S_1 state. The same is clear from Fig. 9; the size of the π-electron lobe on the chlorine atom gets localized in LUMO whereas in HOMO, it is broad and close to the π-electron lobe of the conjugated atoms. The bond angles C8—C7—C2, C8—C7—C6, and C5—C6—Cl 13, C3—C2—Cl 1 increase by 0.945° and 1.931°, respectively in the excited state. All the dihedral angles are either 180° or 0°, reflecting the planarity of the molecule in the ground as well as in the excited state.

From the listed bond lengths and bond angles, it can be clearly seen that 2,6-DCBN tetramer is of good symmetry in the ground state but its symmetrical structure disappears in the electronic excited state. The intermolecular bond lengths N9···H23, N9···H49, N35···H25 and N35···H47 are almost same in the ground state. The lengths of the former three bonds increase from 2.95964 Å, 2.95625 Å and 2.95705 Å to 2.97761 Å, 3.16618 Å and 2.98577 Å respectively upon photoexcitation. At the same time, the bond length N35···H47 is shortened. The calculated results testify that the intermolecular hydrogen bonds N9···H23, N9···H49 and N35···H25 are weakened while the other bond N35···H47 is strengthened in electronic excited state. As demonstrated by Table 7, the intermolecular bonds Cl 1···Cl 50, Cl 26···Cl 27 and Cl 39···Cl 40 are weakened while the bond Cl 13···Cl 14 is strengthened in the S_1 state. The above analysis is supported by the fact that the energy difference of monomer and tetramer in the ground state (−3720.17066 hartree) is greater than that in the excited state (−3720.17105 hartree) ($\Delta E_{GS} > \Delta E_{ES}$). It is well known that the study of molecular orbitals can directly provide insight into the nature of the excited state. Fig. 10 shows the major molecular orbitals involved in electronic transitions using HF/6-31G method. For the hydrogen bonded tetramer, the S_1 state corresponds to HOMO → LUMO transition. It is noted that the electron density of HOMO orbital localize on second and forth unit, while that of LUMO orbital on first and third unit. This indicates that the S_1 state of 2,6-DCBN tetramer is a charge transfer state. A crucial step in the theoretical investigations employing TD-DFT is the choice of an approximate exchange–correlation functional and reasonable basis set. One cannot expect that one approximate functional describes excited states of molecule equally well, especially when different kinds of transitions are present. HOMO–LUMO surfaces have been plotted for the tetramer with different functionals and basis sets B3LYP/6-31G, M062X/6-31G and B3LYP/6-311++G(d,p) as shown in Fig. S6(a)–(c). In all cases, the HOMO → LUMO transition is characterized by intermolecular charge transfer.

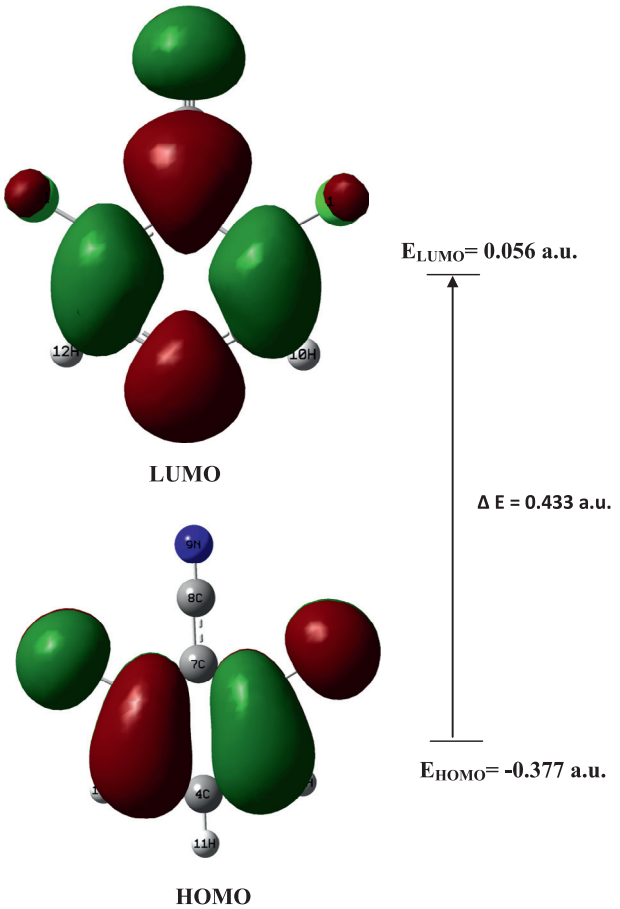

Fig. 9. Frountier molecular orbitals of 2,6-DCBN monomer by HF method using 6-31G basis set.

To depict the excited-state hydrogen bonding dynamics, we calculated the excited-state infrared spectra of 2,6-DCBN monomer as well as tetramer using the TD-DFT method. The calculation of the IR spectra in electronically excited states is difficult and very time-consuming. The IR frequency calculations have been done by HF method using 6-31G basis sets and are given in Table 8 along with those in the ground state. The vibrational spectra of 2,6-DCBN monomer and tetramer both in the ground and excited states in the vibrational regions of C≡N, C—Cl stretching modes and C—H in-plane and out-of-plane bending modes are shown in Fig. 11. The hydrogen bond response upon electronic excitation can be revealed by monitoring the spectral shifts of some characteristic vibrational modes involved in the formation of intermolecular bonds. The C≡N stretching vibrational frequency of 2,6-DCBN monomer in the ground state has been calculated at 2485 cm^{-1}. This mode in the excited state is calculated at 1822 cm^{-1}, which suggests that the electronic excitation induces the C≡N stretching frequency shift to the red. In the infrared spectra of tetramer, one of the frequencies shows downshifting of 603 cm^{-1} on going from ground state to excited state following the increase in the C≡N bond length. It is noted that the bond length of C≡N group of one of the units is lengthened (0.03760 Å), whereas that of other three units show negligible change. It can be seen that the intermolecular hydrogen bonding interaction induces the C≡N stretching mode shift to red by 7 cm^{-1} in ground state and to blue by 53 cm^{-1} in excited state. However, the charge transfer in the excited state induces the C≡N stretching mode of monomer and tetramer shift to red by 663 and 603 cm^{-1} by comparison to C≡N stretching frequencies of their ground states. Therefore, it is concluded that the C≡N stretching mode of 2,6-DCBN is very sensitive to the charge transfer, while less sensitive to the hydrogen bonding interaction.

In the excited state of both monomer and tetramer, the calculated C—H stretching modes show very small change reflecting small effect of excitation on C—H stretching. This is also supported by small changes in bond lengths of C—H as reported in Table 5. However the hydrogen bonding interactions influence the stretching mode of C—H group in ground state as well as in the excited state. A shift of 10–15 cm^{-1} is seen between the monomer and the tetramer. As a result, the stretching mode of C—H group is

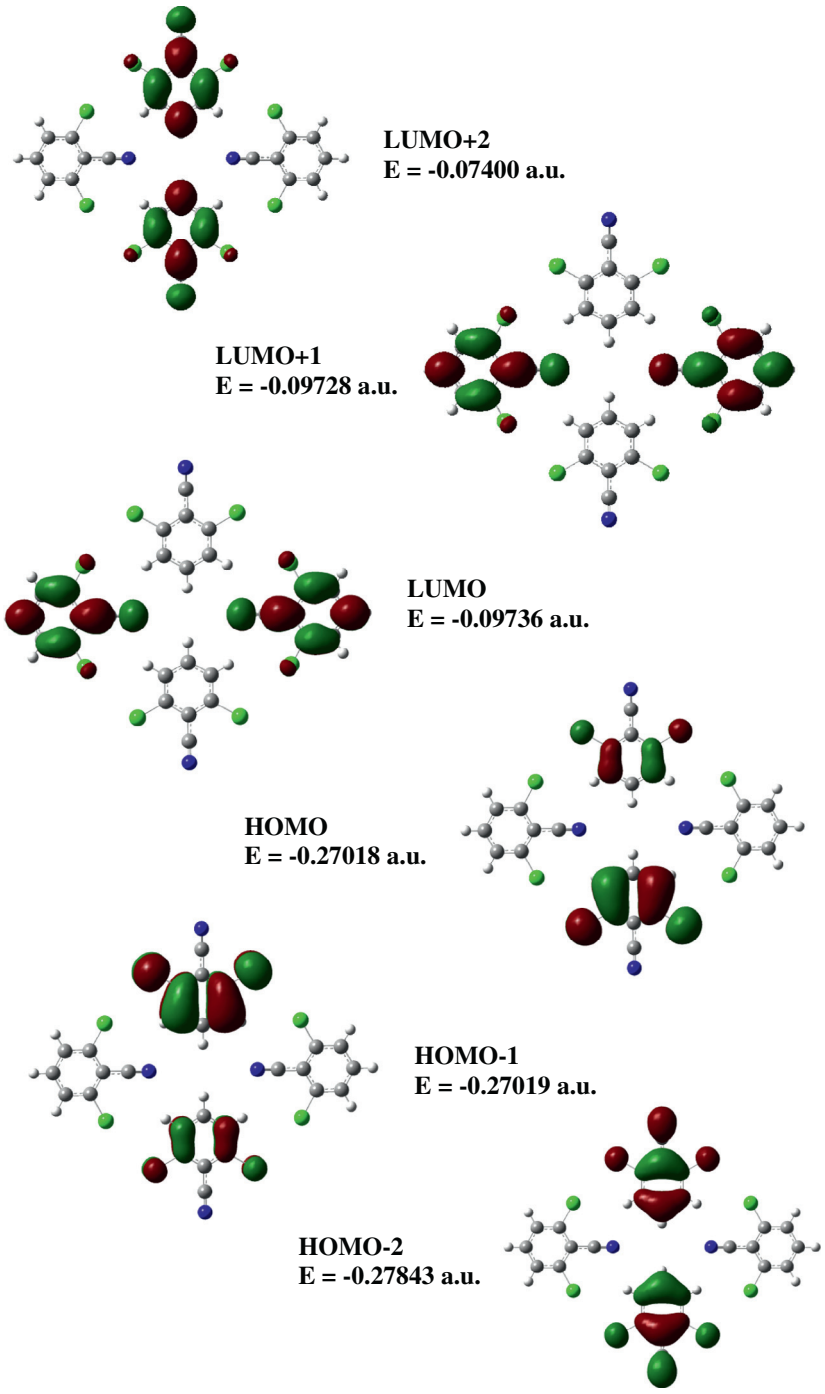

Fig. 10. The atomic orbital compositions of the molecular orbitals of 2,6-DCBN tetramer A with HF/6-31G level.

not a sensitive vibrational mode to monitor the excited state vibrational dynamics.

The C—H in plane bending modes in 2,6-DCBN monomer are calculated in the range 1750–1200 cm^{-1} in the ground state and show red shifting of 100–150 wavenumbers upon photoexcitation to S_1 state. However, in tetramer, the electronic excitation induces relatively smaller red-shifts of 50–100 cm^{-1} in some of the modes while some remain unchanged. In the out of plane bending modes of C—H group, the intermolecular hydrogen bond N···H induces a slight blue shift from 1186, 894 and 638 cm^{-1} in isolated 2,6-DCBN to 1203, 905 and 638 cm^{-1} in the hydrogen-bonded tetramer. These modes are drastically red-shifted by 124, 50 and 75 cm^{-1} upon electronic excitation. Therefore, both the electronic excitation and intermolecular hydrogen bonding interactions can shift the out of plane bending mode of C—H group. However, the hydrogen bonding interactions cannot significantly influence this mode in ground state, in comparison to the electronic excitation.

The C—Cl stretching vibrational frequencies of monomer calculated at 839 and 455 cm^{-1} give downshifting of 788 and 403 cm^{-1} upon electronic excitation. The spectral shift of the C—Cl stretching bands in excited states can be driven by changes of local charge distribution, since the electronic state hopping from ground state to the S_1 state is followed by the intramolecular charge redistribution in the S_1 state of 2,6-DCBN monomer. Upon electronic excitation to

Table 8
Calculated scaled wavenumbers (cm^{-1}) of 2,6-DCBN monomer and tetramer A in ground state and excited state with HF method using 6-31G basis set.

Monomer Ground state	Monomer Excited state	Tetramer A Ground state	Tetramer A Excited state
3262	3261	3274, 3274, 3268, 3268	3273, 3272, 3266, 3266
3256	3253	3263, 3263, 3258, 3258	3263, 3262, 3258, 3254
3255	3241	3255, 3253, 3235, 3235	3254, 3251, 3244, 3235
2485	1822	2482, 2482, 2478, 2478	2482, 2482, 2478, 1875
1758	1610	1756, 1756, 1755, 1754	1756, 1754, 1752, 1723
1723	1608	1723, 1723, 1721, 1720	1720, 1720, 1623, 1609
1594	1441	1595, 1595, 1589, 1588	1595, 1590, 1588, 1587
1589	1437	1587, 1587, 1587, 1587	1586, 1586, 1444, 1440
1355	1402	1358, 1358, 1353, 1351	1396, 1358, 1353, 1351
1330	1303	1329, 1329, 1329, 1329	1329, 1329, 1328, 1324
1306	1244	1307, 1307, 1307, 1306	1307, 1307, 1306, 1273
1271	1145	1272, 1272, 1269, 1265	1269, 1266, 1244, 1208
1207	1111	1209, 1208, 1206, 1203	1206, 1203, 1203, 1202
1186	1062	1203, 1202, 1190, 1190	1190, 1170, 1170, 1170
1171	1047	1170, 1170, 1170, 1170	1153, 1115, 1109, 1107
1096	1022	1107, 1106, 1098, 1098	1098, 1064, 1056, 986
975	844	986, 981, 976. 976	983, 981, 976, 906
894	838	905, 901, 895, 895	902, 895, 861, 860
862	844	861, 861, 860, 859	859, 846, 839, 836
839	788	840, 839, 834, 834	834, 834, 824, 780
670	585	673, 673, 670, 670	673, 670, 670, 652
651	579	652, 652, 651, 650	651, 651, 638, 638
638	526	638, 638, 638, 638	638, 585, 584, 583
585	513	586, 585, 584, 583	580, 563, 527, 510
465	403	470, 469, 468, 467	470, 468, 467, 455
455	371	455, 455, 454, 454	454, 454, 388, 387
387	367	388, 388, 387, 387	386, 386, 385, 385
385	363	386, 386, 385, 385	375, 372, 366, 358
230	211	235, 234, 232, 232	235, 234, 233, 232
230	206	231, 231, 230, 230	231, 230, 217, 214
212	205	214, 214, 213, 212	213, 212, 207, 206
157	149	166, 164, 157, 157	165, 158, 158, 157
91	34	97, 94, 92, 92	96, 92, 92, 60
		41, 36, 29, 27	41, 31, 30, 28
		27, 26, 24, 21	28, 27, 24, 19
		14, 12, 11, 9	17, 13, 11, 9

the S_1 state of hydrogen-bonded tetramer, the C—Cl stretching band continues to downshift from 834, 454 cm^{-1} to 780, 387 cm^{-1}. This means that the intermolecular hydrogen-bonding interactions can induce a larger spectral red shift of the C—Cl stretching band in the excited state than that in the ground state.

The excited-state hydrogen bonding dynamics is dominantly determined by the vibrational motions of the hydrogen donor and acceptor groups, which typically occur on ultrafast time scales of hundreds of femtoseconds. Therefore, to directly monitor the ultrafast dynamical behavior of hydrogen bonds in the excited state, femtosecond time-resolved vibrational spectroscopic techniques are used [70,71]. As no experimental data is available on 2,6 DCBN, we have repeated the calculations with another basis set HF/3-21G in order to check the validity of our results. The optimized structures of monomer and tetramer in the excited state are shown in Fig. S5(a) and (b). The vibrational modes of monomer and tetramer in the ground and the excited states are given in Table S4. Fig. S7 shows the calculated IR spectra for the isolated monomer as well as for the tetramer in the ground and the excited states. We find that similar conclusions can be drawn using this basis set as those with 6-31G.

Thermodynamic properties

Thermodynamic properties, such as heat capacity, entropy and enthalpy, are important parameters in predicting reactive properties of chemical reactions and judge feasibility of different reaction pathways. Results from DFT in the microscopic regime are combined with concepts from Statistical Mechanics for prediction of finite temperature thermodynamic data in macroscopic regime.

The calculations were carried out using the ideal gas approximation at constant pressure equal to 1 atm. The various translational, rotational and vibrational components are used to compute heat capacity (C_p), entropy (S), enthalpy (H) and free energy (G) at finite temperature as shown in table S5. The correlations between these thermodynamic properties and temperatures T are shown in Fig. S8. From the data, it is found that all the thermodynamic functions increase with temperature. The gradient of heat capacity and entropy of tetramer is much higher than that of monomer while it is slightly higher in case of enthalpy. At low temperatures, the main contributions to the heat capacity are from the translations and rotations of molecules while vibrational modes are frozen. At high temperatures, the vibrational movement is intensified, which leads to an increase in the thermodynamic function. The value of heat capacity of tetramer is larger than four times of monomer by an amount ~17 kcal/mol.

The calculated values of entropy indicate that, as the temperature increases, the randomness of the molecules increases. In other words, the gas molecules will be distributed into a greater number of energy levels. At low temperatures, the translational energy levels contribute strongly to the behavior of entropy. Therefore, rotational and vibrational populations are distributed in a few low energy levels. At high temperatures, the vibrational population will be distributed in a larger number of vibrational levels, contributing to increase of entropy.

The enthalpy temperature plot provides information about the total amount of stored energy, mainly in the molecular bonds of the compound, which may be used to analyze chemical reactions between 2,6-DCBN and other compounds. It is evident from the graph that as the temperature increases, the amount of available

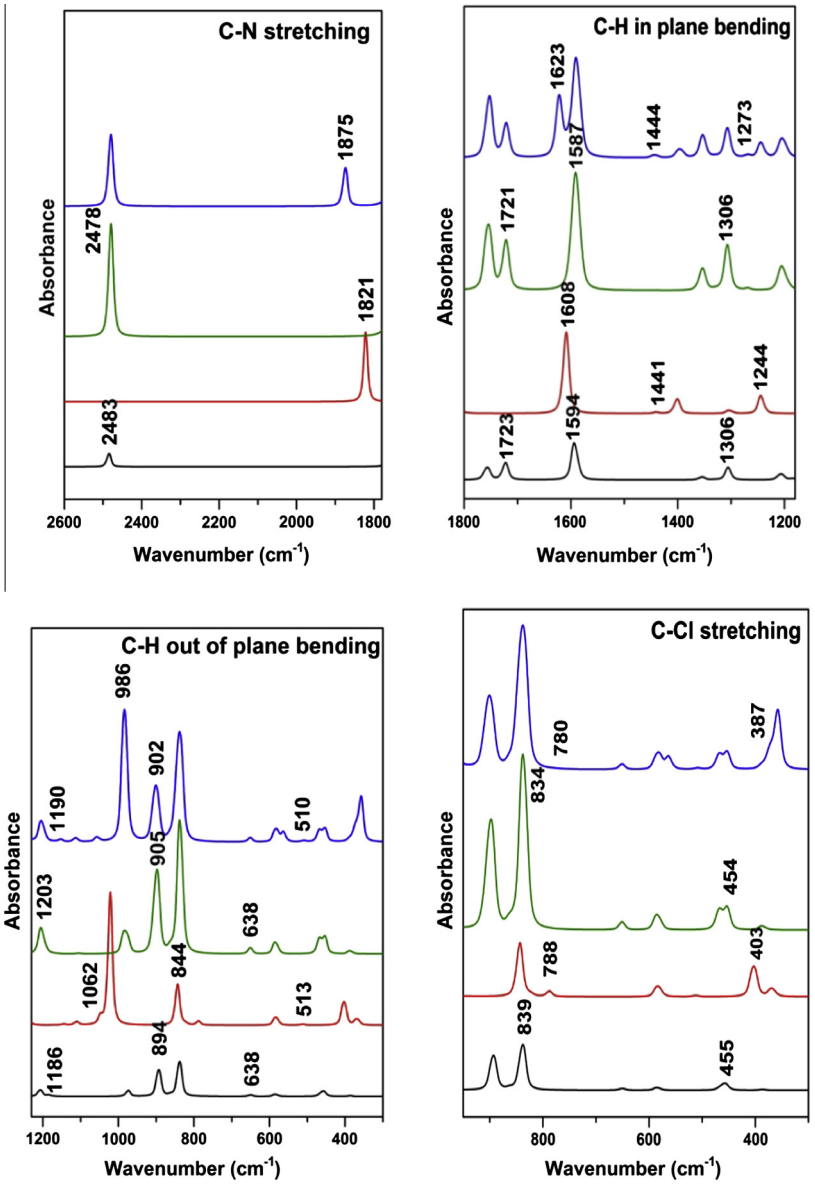

Fig. 11. Theoretically scaled Infrared spectra of monomer and tetramer simulations in ground and excited state using HF/6-31G methods. Black, red represent monomer and Green, blue represent tetramer spectra, in the ground and excited sate respectively. (For interpretation of the references to color in this figure legend, the reader is referred to the web version of this article.)

reaction energy of the compound does too. The enthalpy changes for the tetramerization process are negative throughout the temperature range except in the vicinity of melting point. This finding suggests that the interaction energy between four individual molecules is less enthalpically stabilizing than that between an aggregate and an individual molecule. Hence the formation of tetramer is enthalpically favoured. The tetramerization enthalpies of the 2,6-DCBN become less stabilizing with increase in temperature.

The behavior of the free energy of the system, is consistent with its definition G = H-TS and the performance of state function H and S. The change in Gibb's free energy during the tetramerization process is positive under 500 K. This indicates that the tetramerization process cannot spontaneously occur under 500 K. The ΔG value increases as temperature increases, thus the interactions weaken with the rise in temperature.

The correlation equations for both the monomer and the tetramer are as follows:

For monomer,

$$C_p = 3.1354 + 0.09563T - 4.0214 * 10^{-5}T^2 \quad (R^2 = 0.99995)$$
$$S = 53.4828 + 0.13845T - 5.82429 * 10^{-5}T^2 \quad (R^2 = 0.99987)$$
$$H = 54.8426 + 0.0062T + 3.58786 * 10^{-5}T^2 \quad (R^2 = 0.99997) \tag{7}$$

For tetramer,

$$C_p = 28.6668 + 0.3839T - 1.7005 * 10^{-4}T^2 \quad (R^2 = 0.99997)$$
$$S = 111.8988 + 0.6476T - 3.15514 * 10^{-4}T^2 \quad (R^2 = 0.99976)$$
$$H = 220.14741 + 0.04175T + 1.442 * 10^{-4}T^2 \quad (R^2 = 0.99997) \tag{8}$$

All the thermodynamic data supply helpful information for further studies on 2,6-DCBN. They can be used to compute other thermodynamic parameters according to the relationships of thermodynamic functions and estimate directions of chemical reactions in thermochemical field according to second law of thermodynamics. It should be kept in mind that all thermodynamic calculations were

done in gas phase and they could not be used in solution. The theoretical results presented here could be useful for determining the conditions of synthesis of the new structures, which have not been obtained experimentally till date.

Conclusion

A systematic study has been conducted on the structural and spectral characteristics of 2,6-DCBN in gas phase and in tetramer form by experimental spectroscopic methods and quantum chemical calculations. An effort is made to interpret the changes that occur in the vibrational spectra between the monomer and the tetramer form. The theoretically constructed IR and Raman spectra of the tetramer show good correlation with experimentally observed ones in the solid state. There is a difference between the observed and scaled wavenumber values of the cyano and the chlorine fundamentals of the monomer due to the presence of the intermolecular hydrogen bonding in the solid state. Our simulation with a tetramer form, improves the spectra, but the calculated hydrogen bonds are too weak.

The size, shape, charge density distribution and structure–activity relationship of the 2,6-DCBN molecule was obtained by mapping electrostatic potential surface on the electron density isosurface. Natural bond orbital analysis reflects the charge transfer interaction in the individual hydrogen bond units and the stability of tetramer of DCBN. The UV spectra of 2,6-DCBN have been measured in methanol solution and compared with the theoretical results obtained in the gas phase as well as in the methanol environment using TD-DFT method. The HOMO–LUMO transition clearly explicates the charge transfer interaction in the whole molecular plane. By theoretically monitoring the optimized geometry and the spectral shifts of some characteristic hydrogen-bonding vibrational modes in the excited state, weakening of both the intermolecular hydrogen bonds (N···H, Cl···Cl) upon electronic excitation was predicted for the tetramer. The ^{13}C NMR spectra of the compound were recorded and on the basis of calculated and experimental results, assignments of the chemical shifts were done. The thermodynamic properties of 2,6-DCBN at different temperatures were calculated, revealing the correlations between heat capacity, entropy, enthalpy and temperatures. The interaction energy with basis set superposition error (BSSE) has been estimated using counterpoise method at different levels of theory with various functionals and basis sets. The effects of BSSE on interaction energies and harmonic vibrational wavenumbers are discussed and compared with the existing experimental data.

Acknowledgements

A.G. and P.A. are grateful to University Grants Commission for providing financial assistance under the major research project and Dr. D.S. Kothari Post Doctoral Fellowship. Authors are thankful to Central Drug Research Institute, Lucknow for providing instrumentation facilities for recording UV and NMR spectra of the sample. A thankful acknowledgement is made to Prof. Attila Bende, National Institute of R&D of Isotopic and Molecular Technologies, Cluj-Napoca, Romania for fruitful discussions.

Appendix A. Supplementary material

Supplementary data associated with this article can be found, in the online version, at http://dx.doi.org/10.1016/j.saa.2013.10.104.

References

[1] A.A. Fadda, El-Sayed M. Afsah, R.S. Awad, Eur. J. Med. Chem. 60 (2013) 421–430.
[2] S. Zhang, Y. Zhang, X. Ma, L. Lu, Y. He, Y.J. Deng, J. Phys. Chem. B 117 (9) (2013) 2764–2772.
[3] W. Tan, D. Zhang, H. Wu, D. Zhu, Tetrahedron Lett. 49 (8) (2008) 1361–1364.
[4] L. Peng, L. Zhang, X. Cheng, L.S. Fan, H.Q. Hao, Plant Biol. 15 (2013) 405–414.
[5] J.A. Butera, M.M. Antane, S.A. Antane, T.M. Argentieri, C. Freeden, R.F. Gracetta, B.H. Hirtu, D. Jenkins, J.R. Lennors, E. Matelan, N.N. Norton, D. Quagliato, J.H. Sheldon, W. Spinell, D. Warga, A. Wojdan, M.J. Woods, Med. Chem. 43 (6) (2000) 1187–1203.
[6] S.L. Cheav, S. Kirkiacharian, F. Pieri, O. Poimon, Ann. Pharm. Fr. 56 (1998) 205–208.
[7] E. Björklund, B. Styrishave, G.G. Anskjær, M. Hansen, B.H. Sørensen, Sci. Total. Environ. 409 (19) (2011) 3732–3739.
[8] C. Cox, J. Pestic. Ref./Spring 17 (1) (1997) 14–20.
[9] S. DeBolt, R. Gutierrez, D.W. Ehrhardt, C. Somerville, Plant Physiol. 145 (2007) 334–338.
[10] Z. Qiong, H. Chi, X. Chongwen, H. Qiyong, (1997) (CN 1166378 A).
[11] S. Sudha, N. Sundaraganesan, M. Kurt, M. Cinar, M. Karabacak, J. Mol. Struct. 985 (2011) 148–156.
[12] A.R. Krishnan, H. Saleem, S. Subashchandrabose, N. Sundaraganesan, S. Sebastain, Spectrochim. Acta A 78 (2011) 660–669.
[13] V.K. Rastogi, M.A. Palafox, R. Tomar, U. Singh, Spectrochim. Acta A 110 (2013) 458–470.
[14] P. Agarwal, N. Choudhary, A. Gupta, P. Tandon, Vib. Spectrosc. 64 (2013) 134–147.
[15] A. Gupta, S. Bee, N. Choudhary, S. Mishra, P. Tandon, Mol. Simul. 38 (7) (2012) 567–681.
[16] N. Choudhary, S. Bee, A. Gupta, P. Tandon, Comput. Theor. Chem. 1016 (2013) 8–21.
[17] S. Bee, P. Agarwal, A. Gupta, P. Tandon, Spectrochim. Acta A 114 (2013) 236–255.
[18] M.J. Frisch, G.W. Trucks, H.B. Schlegel, G.E. Scuseria, M.A. Robb, J.R. Cheeseman, J.A. Montgomery, Jr., T. Vreven, K.N. Kudin, J.C. Burant, J.M. Millam, S.S. Iyengar, J. Tomasi, V. Barone, B. Mennucci, M. Cossi, G. Scalmani, N. Rega, G.A. Petersson, H. Nakatsuji, M. Hada, M. Ehara, K. Toyota, R. Fukuda, J. Hasegawa, M. Ishida, T. Nakajima, Y. Honda, O. Kitao, H. Nakai, M. Klene, X. Li, J.E. Knox, H.P. Hratchian, J.B. Cross, C. Adamo, J. Jaramillo, R. Gomperts, R.E. Stratmann, O. Yazyev, A.J. Austin, R. Cammi, C. Pomelli, J.W. Ochterski, P.Y. Ayala, K. Morokuma, G.A. Voth, P. Salvador, J.J. Dannenberg, V.G. Zakrzewski, S. Dapprich, A.D. Daniels, M.C. Strain, O. Farkas, D.K. Malick, A.D. Rabuck, K. Raghavachari, J.B. Foresman, J.V. Ortiz, Q. Cui, A.G. Baboul, S. Clifford, J. Cioslowski, B.B. Stefanov, G. Liu, A. Liashenko, P. Piskorz, I. Komaromi, R.L. Martin, D.J. Fox, T. Keith, M.A. Al-Laham, C.Y. Peng, A. Nanayakkara, M. Challacombe, P.M.W. Gill, B. Johnson, W. Chen, M.W. Wong, C. Gonzalez, J.A. Pople, Gaussian 03, Revision C.02, Gaussian Inc., Wallingford, CT 06492, 2004.
[19] T. Vladimiroff, J. Mol. Struct. (Theochem.) 453 (1998) 119–122.
[20] C.T. Lee, W.T. Yang, R.G. Parr, Phys. Rev. B 37 (1988) 785–789.
[21] R.G. Parr, W. Yang, Density Functional Theory of Atoms and Molecules, Oxford University Press, New York, 1989.
[22] A.D. Becke, J. Chem. Phys. 98 (1993) 5648–5652.
[23] P.J. Stephens, F.J. Devlin, C.F. Chabalowski, M.J. Frisch, J. Phys. Chem. 98 (1994) 11623–11627.
[24] G. Keresztury, J.M. Chalmers, P.R. Griffith, Raman Spectroscopy: Theory, Hand Book of Vibrational Spectroscopy, vol. 1, John Wiley & Sons Ltd., New York, 2002.
[25] G. Keresztury, S. Holly, J. Varga, G. Besenyei, A.Y. Wang, J.R. Durig, Spectrochim. Acta A 49 (1993) 2007–2026.
[26] J.M.L. Martin, C.V. Alsenoy, Gar2ped, University of Antwerp, Antiwerp, 1995.
[27] P. Pulay, G. Fogarasi, F. Pang, J.E. Boggs, J. Am. Chem. Soc. 101 (1979) 2550–2560.
[28] G. Fogarasi, X. Zhou, P.W. Taylor, P. Pulay, J. Am. Chem. Soc. 114 (1992) 8191–8201.
[29] A. Frisch, A.B. Nielson, A.J. Holder, Gauss View User Manual, Gaussian Inc., Pittsburgh, PA, 2000.
[30] M. Karabacak, M. Cinar, M. Kurt, J. Mol. Struct. 885 (2008) 28–35.
[31] H. Yoshida, K. Takeda, J. Okamura, A. Ehara, H. Matsurra, J. Phys. Chem. A 106 (2002) 3580–3586.
[32] D. Britton, W.E. Noland, M.J. Pinnow, Acta Cryst. B56 (2000) 822–827.
[33] S.D. Sharma, S. Doraiswamys, J. Mol. Spectosc. 180 (1) (1996) 7–14.
[34] M. Onda, M. Atsuki, J. Yamaguchi, K. Suga, I. Yamaguchi, J. Mol. Struct. 295 (1993) 101–104.
[35] V.K. Rastogi, M.A. Palafox, S. Singhal, S.P. Ojha, W. Kiefer, Int. J. Quant. Chem. 107 (5) (2007) 1099–1114.
[36] E.D. Glendening, A.E. Reed, J.E. Carpenter, F. Weinhold, NBO 3.0 Program Manual, Theoretical Chemistry Institute, University of Wisconsin, Madison, Wisconsin, 1990.
[37] A.E. Reed, L.A. Curtiss, F. Weinhold, Chem. Rev. 88 (1988) 899–926.
[38] J.S. Murray, K. Sen (Eds.), Molecular Electrostatic Potentials: Concepts and Applications, Theoretical and Computational Chemistry, Vol. 3, Elsevier Science, 1996.
[39] M.H. Griffiths, J.A. Moss, J.A. Rose, D.E. Hathway, Biochem. J. 98 (1966) 770–781.
[40] R. Ditchfield, Mol. Phys. 27 (1974) 789–807.
[41] K. Wolinski, J.F. Hinton, P. Pulay, J. Am. Chem. Soc. 112 (23) (1990) 8251–8260.
[42] V. Arjunan, K. Carthigayan, S. Periandy, K. Balamurugan, S. Mohan, Spectrochim. Acta Part A: Mol. Biomol. Spectrosc. 98 (2012) 156–169.

[43] Y. Sert, C. Cırak, F. Ucun, Spectrochim. Acta Part A: Mol. Biomol. Spectrosc. 107 (2013) 248–255.
[44] M. Arivazhagan, R. Meenakshi, S. Prabhakaran, Spectrochim. Acta Part A: Mol. Biomol. Spectrosc. 102 (2013) 59–65.
[45] G. Socrates, Infrared and Raman Characteristic Group Frequencies, third ed., John Wiley & Sons Ltd., Chichester, 2001.
[46] G. Socrates, Infrared and Raman Characteristic Group Frequencies, third ed., John Wiley & Sons Ltd., Chichester, 2001.
[47] M. Alcolea Palafox, V. Bena Jothy, Surabhi Singhal, I. Hubert Joe, Satendra Kumar, V.K. Rastogi, Spectrochim. Acta Part A Mol. Biomol. Spectrosc. 116 (2013) 509–517.
[48] V.K. Rastogi, V. Jain, M.A. Palafox, D.N. Singh, R.A. Yadav, Spectrochim. Acta Part A Mol. Biomol. Spectrosc. 57 (2001) 209–216.
[49] B. Smith, Infrared Spectral Interpretation, A Systematic Approach, CRC Press, Washington, DC, 1999.
[50] D.L. Vien, N.B. Colthup, W.G. Fateley, J.G. Grasselli, The Handbook of Infrared and Raman Characterstic Frequencies of Organic Molecules, Academic Press Inc., San Diego California, 1991.
[51] S. Jeyavijayan, M. Arivazhagan, Spectrochim. Acta Part A 81 (2011) 466–474.
[52] A.R. Krishnan, H. Saleem, S. Subashchandrabose, N. Sundaraganesan, S. Sebastain, Spectrochim. Acta Part A 78 (2011) 582–589.
[53] V.K. Rastogi, M. Alcolea Palafox, Rashmi Tomar, Upama Singh, Spectrochim. Acta Part A Mol. Biomol. Spectrosc. 110 (2013) 458–470.
[54] S. Dheivamala, V. Silambarasan, Spectrochim. Acta Part A Mol. Biomol. Spectrosc. 96 (2012) 480–484.
[55] B. Lakshmaiah, G. Ramana Rao, J. Raman Spectrosc. 20 (1989) 439.
[56] O. Alver, Z. Hayvalı, H. Guler, H. Dal, M. Senyel, J. Mol. Struct. 991 (2011) 12–17.
[57] V.K. Rastogi, M.A. Palafox, R.P. Tanwar, L. Mittal, Spectrochim. Acta A 58 (2002) 1987–2004.
[58] E.F. Mooney, Spectrochim. Acta A 20 (1964) 1343–1348.
[59] S. Sudha, N. Sunderganesan, M. Kurt, M. Cinar, M. Karabacak, J. Mol. Struct. 985 (2011) 148–156.
[60] A.R. Krishnan, H. Saleem, S. Subashchandrabose, N. Sunderaganesan, S. Sebastain, Spectrochim. Acta A 78 (2011) 582–589.
[61] N.P.G. Roeges, A Guide to the Complete Interpretation of Infrared Spectra of Organic Structures, John Wiley & Sons, New York, 1994.
[62] S.F. Boys, F. Bernardi, Mol. Phys. 19 (1970) 553–566.
[63] N.X. Wang, K. Venkatesh, A.K. Wilson, J. Phys. Chem. A 110 (2006) 779–784.
[64] Y. Zhao, D. Truhlar, Theor. Chim. Acta 120 (1) (2008) 215–241.
[65] P. Hobza, V. Spirko, Phys. Chem. Chem. Phys. 5 (2003) 1290–1294.
[66] E. Runge, E.K.U. Gross, Phys. Rev. Lett. 52 (1984) 997–1000.
[67] M.E. Casida, K.C. Casida, D.R. Salahub, Int. J. Quant. Chem. 70 (1998) 933–941.
[68] E. Cances, B. Mennucci, J. Tomasi, J. Chem. Phys. 107 (1997) 3032–3041.
[69] M. Cossi, G. Scalmani, N. Rega, V. Barone, J. Chem. Phys. 117 (2002) 43–54.
[70] G.-J. Zhao, K.-L. Han, J. Phys. Chem. A 111 (2007) 9218–9223.
[71] G.-J. Zhao, K.-L. Han, J. Phys. Chem. A 113 (2009) 14329–14335.